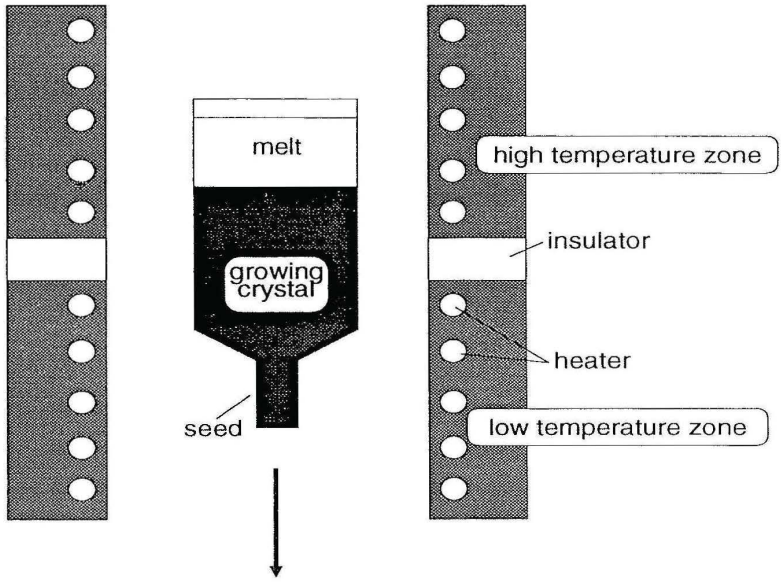

Fig. 9.6. Crystal growth according to the Bridgman-Stockbarger method

[17]. CsI : Tl crystals up to several inches in diameter can be grown out of quartz ampoules, but today Pt crucibles are used for the growth of all alkali halides.

Crystals of BaF_2 as well as CeF_3 can also be grown by the Bridgman-Stockbarger method.

The elements of the Czochralski technique are shown schematically in Fig. 9.7. The melt is contained in the crucible which is heated either by radio-frequency-induction heating or by resistance heating. The pull rod with a chuck containing the seed crystal at its lower end is positioned axially above the crucible. The seed crystal is dipped into the melt and the melt temperature adjusted until the meniscus is supported. The pull rod is rotated slowly and then lifted. By careful adjustment of the power supplied to the melt, the diameter of the crystal is controlled as it grows. Rotation rates are commonly in the range of 1–100 rpm. Pulling rates can vary from one millimeter per hour for certain oxide crystals to several tens of millimeters per hour for halide crystals. The whole assembly is enclosed within an envelope which permits control of the ambient gas. The principal advantages of the technique include the fact that the crystal remains unstrained when it cools, so that a high structural perfection can be obtained. To yield material of high and controllable purity, it is necessary to fabricate the crucible from a material which is not attacked by the molten charge.

For oxide crystals like $Bi_4Ge_3O_{12}$ (T_m: 1044°C) and $CdWO_4$ (T_m: 1272°C) Pt crucibles are normally used. For crystals with a higher melting temperature, such as Gd_2SiO_5 : Ce (T_m: 1950°C), Ir crucibles are applied [18].

Oxide crystals are usually grown by the Czochralski technique, but alkali halide crystals can also be grown by this method. The perfection of these crystals is high, but the size is normally limited to 3–4 inches diameter. However, with a special

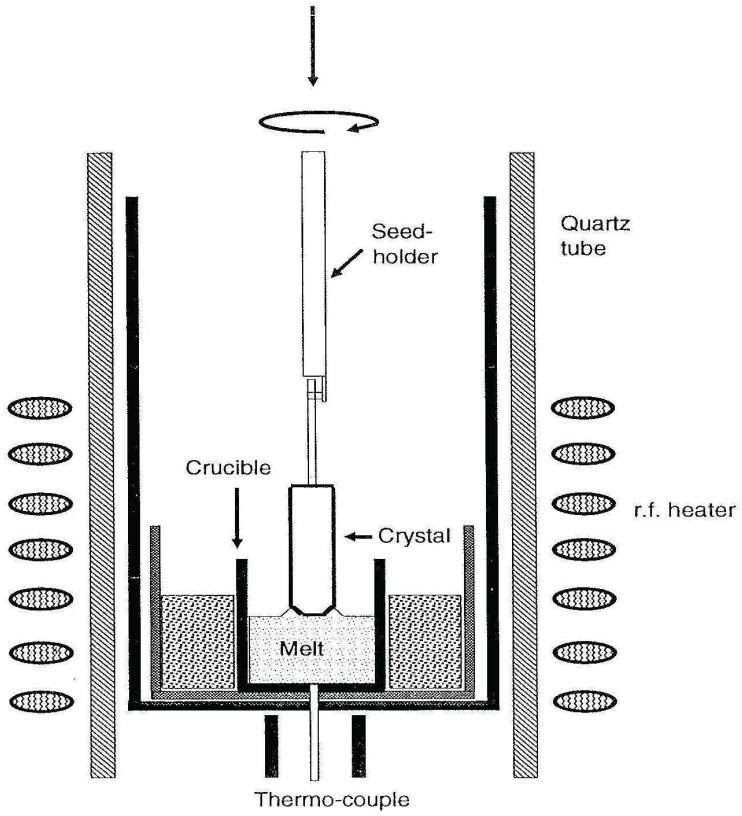

Fig. 9.7. Crystal growth according to the Czochralski method

technique, viz. simultaneous feeding of the starting material during the crystal growth process, perfect halide crystals with up to 20 inches (50 cm) diameter have been grown with a length up to 75 cm [19].

$Bi_4Ge_3O_{12}$ crystals will only be really colorless when the raw materials Bi_2O_3 and Ge_2O have a high purity (5–6N). The growth atmosphere has to be oxygen, otherwise the Pt crucible will be attacked.

The tendency of $Bi_4Ge_3O_{12}$ crystals to grow with a "core" can be partly prevented by application of a higher rotation rate up to 100 rpm. But this inconvenience can be avoided using other growth techniques. Indeed the horizontal Bridgman-Stockbarger method has quite recently become popular for $Bi_4Ge_3O_{12}$ growth, especially in China [20]. The details as to how this technique is applied are not known, but it must be successful. High quality crystals of dimensions $30 \times 30 \times 240$ mm^3 have been obtained, and are, for example applied in electromagnetic calorimeters. In order to grow large stoichiometric single crystals of $CdWO_4$ with a diameter of 3 inches, the Czochralski technique has to be slightly modified to prevent the evaporation of cadmium at the melting point of $CdWO_4$.

Table 9.5. Some properties of scintillators based on alkali halides [4,9,26]

Property	NaI : Tl^+	CsI : Tl^+	CsI : Na	CsI
density (g cm^{-3})	3.67	4.51	4.51	4.51
emission maximum (nm)	415	560	420	315
light yield (photons MeV^{-1})	40.000	55.000	42.000	2.000
decay time (ns)	230	1000	630	16
afterglow (% after 6 ms)	0.3-5	0.5-5	0.5-5	–
stability	hygro-scopic	hygro-scopic	hygro-scopic	hygro-scopic
mechanical behavior	brittle	deform-able	deform-able	deform-able

The large anisotropy of the thermal expansion along the [010] axis of Gd_2SiO_5 : Ce makes the growth of single crystals rather difficult. Cracks due to cooling down from about 1950°C to room temperature occur because of large residual stresses in the grown crystal. But up to now crystals up to 2 inches in diameter have been obtained without cracks. The topics of crystal growth have been treated in many review papers and books [21–24]. As an illustration of what can be achieved today, Fig. 9.8 shows several $Bi_4Ge_3O_{12}$ crystals. Two freshly-grown ingots without cores are shown, together with several machined crystals.

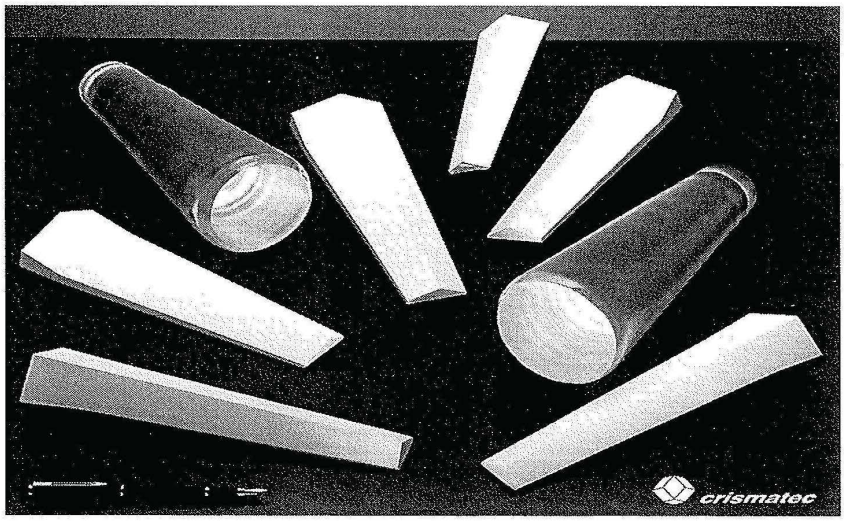

Fig. 9.8. Crystals of $Bi_4Ge_3O_{12}$ grown by the Czochralski method. Two freshly grown ingots as well as several machined crystals are shown. The authors are grateful to the Crismatex Company who made this photograph available

9.5 Scintillator Materials

9.5.1 Alkali Halides

Two of the alkali halides have been used as a scintillator material, viz. NaI and CsI, both doped with Tl^+. Table 9.5 summarizes some of their properties. Also included are CsI : Na and undoped CsI. The emission spectra of the Tl^+-doped crystals are given in Fig. 9.9.

These materials have a very high light yield (except for undoped CsI). For NaI : Tl^+, for example, the radiant efficiency calculated from the light yield is about $\frac{2}{3}$ of the maximum possible efficiency (see Table 9.4). The low light yield of CsI is, certainly for a part, due to thermal quenching [26]. For certain applications the decay time of these scintillators (< 1 μs) is acceptable. Unfortunately the afterglow is considerable and the stability poor. It depends on the application whether these scintillators can be applied or not (see Table 9.3). NaI : Tl^+ is probably the most extensively used scintillator.

The emission of the Tl^+-doped alkali halides is due to the $^3P_1$–$^1S_0$ transition on the Tl^+ ion (see Sect. 3.3.7). It is usually assumed that the afterglow is due to hole trapping in the host lattice (trapped exciton, see Sect. 3.3.1), whereas the electron is trapped by the activator. In CsI : Na the emission is due to an exciton bound to a Na^+ ion, in CsI to self-trapped exciton emission.

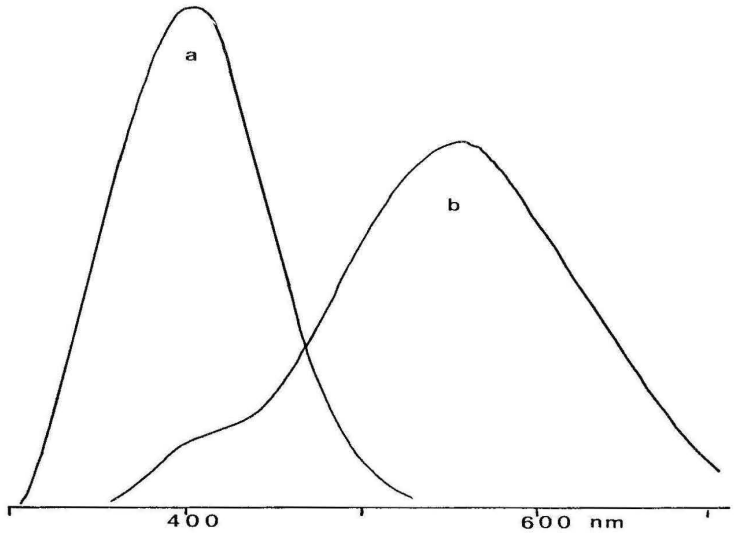

Fig. 9.9. The emission spectra of NaI : Tl (*a*) and CsI : Tl(*b*) at room temperature under X-ray excitation

Table 9.6 Some properties of the tungstate scintillators and $Bi_4Ge_3O_{12}$ [4,9,26]

Property	$ZnWO_4$	$CdWO_4$	$Bi_4Ge_3O_{12}$
density (g cm^{-3})	7.87	7.99	7.13
emission maximum (nm)	480	480	480
light yield (photons MeV^{-1})	10.000	14.000	9.000
decay time (ns)	5000	5000	300
afterglow (% after 3 ms)	< 0.1	< 0.1	0.005
stability	good	good	good
mechanical behavior	brittle	brittle	brittle

9.5.2 Tungstates

The scintillators $ZnWO_4$ and $CdWO_4$ have high densities (see Table 9.6). Their light yields are lower than for the alkali halides, but their afterglow is weak. The crystals cleave easily which makes machining difficult. $CdWO_4$ is toxic.

Their maximum efficiencies can be expected to be below 10% (Sect. 4.4). From the data in Table 9.6, $CdWO_4$ is estimated to yield 3.5%.

These tungstates show broad band emissions originating from the tungstate octahedron (in contradistinction with the scheelite $CaWO_4$, they have the wolframite crystal structure). This type of luminescence was treated in Sect. 3.3.5.

9.5.3 $Bi_4Ge_3O_{12}$ (BGO)

Some properties of BGO are summarized in Table 9.6. It is a very interesting material from the fundamental as well as from the applied point of view. It is used in calorimeters and PET scanners. The decay time is rather short, the afterglow weak, and the density high. Weber [27] has reviewed the history and properties of this scintillator. Figure 9.10 gives the luminescence spectra. The relevant optical transitions were discussed in Sects. 3.3.7 and 5.3.2.

Due to the large Stokes shift of the emission, i.e. the large relaxation in the excited state, the emission of $Bi_4Ge_3O_{12}$ is for the greater part quenched at room temperature. The calculated η_{max} is 6%, but should be reduced to 2% in view of this quenching. The actual value calculated from the data in Table 9.6 is 2%. This shows that, apart from the quenching, there are not many radiationless losses.

The compound $Bi_2Ge_3O_9$ [28] shows similar luminescence properties [29,30]. The Stokes shift is even larger than in $Bi_4Ge_3O_{12}$ (20 000 vs 17 500 cm^{-1}, respectively). As a consequence the emission intensity is quenched at 150 K, making the material unsuitable for application.

The compound $Bi_4Si_3O_{12}$ shows luminescence properties which are very similar to those of the germanium analogue [31,32].

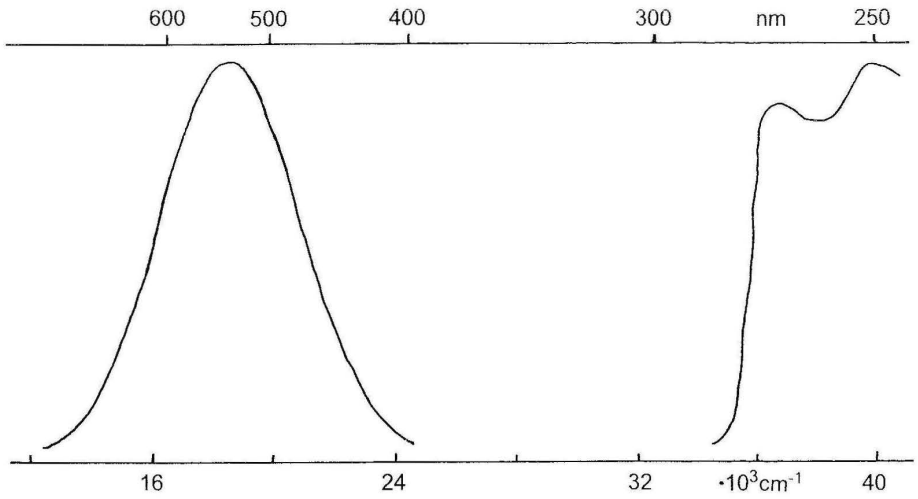

Fig. 9.10. The emission (left) and excitation (right) spectra of the luminescence of $Bi_4Ge_3O_{12}$

Table 9.7. Some properties of Ce^{3+}-activated scintillators [9,26]

Host lattice	Ce^{3+} conc. (mole %)	emission max. (nm)	light yield (photons MeV^{-1})	decay time (ns)	density (g cm^{-3})
BaF_2	0.2	310, 325	7000	60[b]	4.89
LaF_3	10	290, 305	900	27	5.89
CeF_3	100	310, 340	4000	30	6.16
$YA1O_3$	0.1	350, 380	17.000	30	5.55
Gd_2SiO_5	0.5	440	9000	60[b]	6.71
Lu_2SiO_5[a]		420	25.000	40	7.4
glass[c]	4	390	1500	70[b]	2.5
$Y_3Al_5O_{12}$	0.4	550	14.000	65	5

a C.L. Melcher, p. 415 in Ref. 1

b and longer component

c composition $(SiO_2)_{0.55}(MgO)_{0.24}(Al_2O_3)_{0.06}(Li_2O)_{0.06}(Ce_2O_3)_{0.04}$

9.5.4 $Gd_2SiO_5 : Ce^{3+}$ and $Lu_2SiO_5 : Ce^{3+}$

The compound Gd_2SiO_5 has a complicated crystal structure with two crystallographic sites for the rare earth ions. In recent years it has become popular as a scintillator. Crystals can be grown with the Czochralski method [19,24]. Their properties are summarized in Table 9.7. It is not hygroscopic, but it cleaves easily which can be a problem for certain applications.

The luminescence of Ce^{3+} was treated in Sects. 3.3.3 and 5.3.2. The emission transition ($5d \rightarrow 4f$) is fully allowed, so that short decay times can be ex-

pected. This is actually observed (see Table 9.7). The variation of the decay time is mainly determined by the emission wavelength according to the relation $\tau \sim \lambda^2$ (see Sect. 3.3.3.a). The light yield of $Gd_2SiO_5:Ce^{3+}$, although not low, is below that expected ($\eta_{observed} \sim 2.5\%$, $\eta_{max} \sim 8\%$).

Suzuki et al. [33] have reported on the ultraviolet and γ-ray excited luminescence of $Gd_2SiO_5:Ce^{3+}$. At 11 K they were able to find luminescence from two different Ce^{3+} ions, one with an emission maximum at about 425 nm, the other with an emission maximum at about 500 nm. The respective lowest excitation bands have their maximum at 345 and 380 nm, and the respective decay times are 27 and 43 ns. The former luminescence is hardly quenched at room temperature, the intensity of the latter decreases above 200 K, and at room temperature only 20% is left. Under γ-ray excitation at room temperature the luminescence is dominated by the 425 nm emission, since the other is quenched for the greater part. Peculiarly enough, the decay shows under these conditions a long component ($\tau \sim 600$ ns) which is not observed for $Y_2SiO_5:Ce^{3+}$ and $Lu_2SiO_5:Ce^{3+}$.

The results of previous chapters of this book allow us to propose a simple explanation for these experimental observations. First we note that the ratio of the decay times (~ 0.65) is about equal to the squared ratio of the emission band maxima (~ 0.75) as is to be expected from $\tau \sim \lambda^2$ (see Sect. 3.3.3a).

The long decay component of $Gd_2SiO_5:Ce^{3+}$ can be ascribed to the fact that part of the electron-hole pairs formed by γ-ray irradiation are captured by Gd^{3+} ions. The excitation energy migrates over the Gd^{3+} ions as described in Sect. 5.3.1. In this way the Ce^{3+} ions are populated in a delayed way, so that a long decay component is observed. This effect does not occur in $Y_2SiO_5:Ce^{3+}$ or $Lu_2SiO_5:Ce^{3+}$, since the host lattice ions do not have energy levels below the band gap energy.

The crystal structure of Gd_2SiO_5 shows that one Ce^{3+} ion is coordinated by 8 oxygen ions belonging to silicate tetrahedra and 1 oxygen which is not bounded to silicon. The latter oxygen is coordinated tetrahedrally by four rare earth ions. The other Ce^{3+} ion is coordinated by 4 oxygen ions belonging to silicate tetrahedra and 3 oxygen ions which are not. The latter Ce^{3+} ion is more strongly covalently bonded, because the oxygen ions without silicon neighbors do not have enough positive charge in their immediate surroundings to compensate their twofold negative charge [34]. Consequently, this Ce^{3+} ion has its energy levels at lower energy (see Sect. 2.2), as has also been observed for Tb^{3+} in Gd_2SiO_5 [34].

Finally the lower quenching temperature of this Ce^{3+} emission remains to be explained. It is important to note that the oxygen ions, coordinated by four rare earth ions only, form a two-dimensional network in the crystal structure of Gd_2SiO_5. The longer-wavelength emitting Ce^{3+} ions are located in this network. There is a striking structural analogy with the structure of Y_2O_3 where every oxygen is tetrahedrally coordinated by 4 yttrium ions, so that here the network is threedimensional. Actually Ce^{3+} in Y_2O_3 does not luminesce due to photoionization (see Sect. 4.5). Also in $Ca_4GdO(BO_3)_3$ the Ce^{3+} ion does not luminesce [35]. In this host lattice a similar structural network can be distinguished. Therefore we conclude that the low quenching temperature of the Ce^{3+} ion in Gd_2SiO_5 which is coordinated by three oxygen ions which do not coordinate to silicon must be explained in the same way.

The quenching of one of the two Ce^{3+} centres in Gd_2SiO_5 is at least partly responsible for the discrepancy between the observed and theoretical values of the efficiency.

The host lattice Lu_2SiO_5 has a different crystal structure which is also the structure of Y_2SiO_5. Luminescence studies do not show a large amount of quenching of the Ce^{3+} emission at room temperature [33]. It is therefore not surprising that in this structure much higher yields can be obtained than in Gd_2SiO_5. The experimental values are close to the theoretical maximum (see Table 9.4). It has been found that $Y_2SiO_5 : Tb^{3+}$ yields, under X-ray excitation, also a higher efficiency than $Gd_2SiO_5 : Tb^{3+}$ [34]. This suggests that the Gd_2SiO_5 structure contains in some way centers which compete with the activator ions for the capture of charge carriers. The scintillator $Lu_2SiO_5 : Ce^{3+}$ seems, therefore, to have many advantages. Unfortunately, the cost price of pure Lu_2O_3 is extremely high.

9.5.5 CeF_3

Some properties of CeF_3 scintillators are gathered in Table 9.7. This material is one of the serious candidates for a new generation of high-precision electromagnetic calorimeters to be used for the new large proton collider to be built at CERN (Geneva). For that purpose one needs a total crystal volume as large as 60 m^3 [2], which is nearly two orders of magnitude more than at present (1.2 m^3 $Bi_4Ge_3O_{12}$). As mentioned, the relatively low light yield of CeF_3 is not detrimental for this specific application (see Table 9.3). In view of these plans, a large amount of research has already been performed on CeF_3 [36–38]. In passing, it should be mentioned that the high costs of this proposal have forced the scientists involved to look for a cheaper solution based on a reasonable compromise between cost and performance.

CeF_3 is a material with 100% activator concentration. As argued in Sect. 5.3.2, the large Stokes shift of the Ce^{3+} emission localizes the excited state, so that concentration quenching by energy migration does not occur.

In our opinion the paper by Moses et al. [36] on the scintillation mechanisms in CeF_3 is a fine example of how scintillators should be studied from a fundamental point of view. A combination of techniques was used, viz. (time-resolved) luminescence spectroscopy, ultraviolet photoelectron spectroscopy, transmission spectroscopy, and the excitation region was extended up to tens of eV by using synchrotron radiation. Further, powders as well as crystals with composition $La_{1-x}Ce_xF_3$ were investigated.

The emission depends strongly on the value of x and on the excitation energy (see also Fig. 9.11). The intrinsic Ce^{3+} emission consists of a narrow band with maxima at 284 and 300 nm. These are ascribed to transitions from the lowest level of the $5d$configuration to the two levels of the $4f$ground configuration ($^2F_{5/2}$, $^2F_{7/2}$) (Sect. 3.3.3). If $x > 0.1$, an additional emission band appears at longer wavelength (around 340 nm) which sometimes even dominates (see Fig. 9.11). This one is ascribed to Ce^{3+} ions close to defects.

Instructive is the emission for $x < 0.01$: it consists of the intrinsic Ce^{3+} emission band, Pr^{3+} emission lines, and a broad band extending from 250 to 500 nm which is ascribed to self-trapped exciton (STE) emission from the host. The STE consists

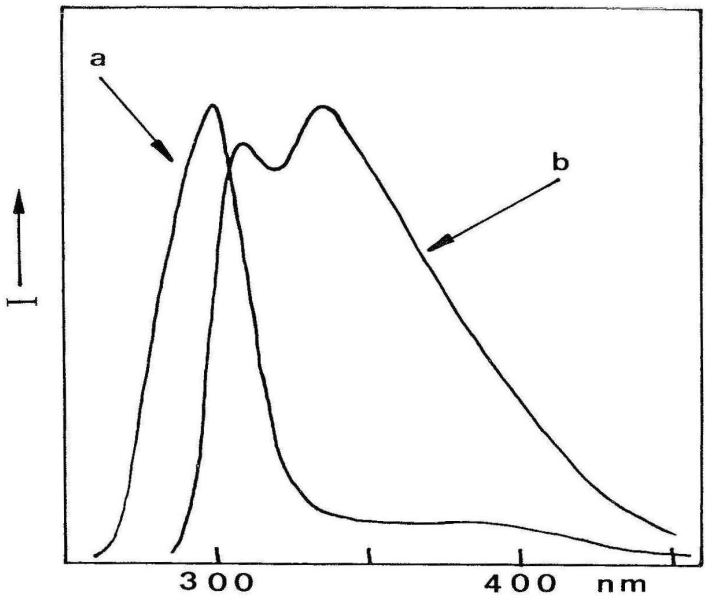

Fig. 9.11. Emission spectra of CeF_3. Curve *a* is for a powder under X-ray excitation, curve *b* for a crystal under γ-ray excitation. From data in Ref. [36]

of an electron bound to a V_K centre which is a hole trapped by two fluorine ions forming a pseudo-molecule F_2^- (Sect. 3.3.1). This shows that the lattice itself also traps the electron-hole pairs. At room temperature the STE migrates over the lattice, ending its life by radiative recombination, transfer to Ce^{3+} or to Pr^{3+} (the latter being present as an impurity), or by nonradiative recombination. This illustrates that for this composition the factor S in Eq. (4.6) is far from one if one considers the Ce^{3+} emission.

In CeF_3 energy transfer (Chapter 5) from intrinsic to extrinsic Ce^{3+} ions takes place [36,37]. Extrinsic Ce^{3+} ions are Ce^{3+} ions near to imperfections in the crystal lattice. Radiative as well as nonradiative transfer contributes. Actually the 340 nm emission shows a build-up which is equal to the decay of the 290 nm emission. The decay times of these emissions are about 30 and 20 ns, respectively. This agrees well with the $\tau \sim \lambda^2$ relation (Sect. 3.3.3a).

Under high-energy excitation an initial much faster decay has been observed. This phenomenon was studied by Pédrini et al. [37]. This fast component is of greater importance if there are more defects (impurities) in the lattice. However, even in very pure crystals it is present. When a high-energy particle is absorbed, the region of its relaxation has a radius of 10–100 nm. Therefore the electronic excitation is correlated in space and time. Auger relaxation in excited pairs has been proposed as a loss mechanism. The importance of this process decreases with temperature, since the excited states become more and more mobile at higher energies, so that the pair of excited ions can dissociate.

The light yield of CeF_3 is low, viz. 4000 photons MeV^{-1}. This corresponds to $\eta \sim 1\%$, whereas $\eta_{max} \sim 8\%$. This shows that the greater part of the emission is quenched. It is usually admitted that impurity rare earth ions cannot be responsible for such a loss. However, fluoride crystals will always contain a certain (low) amount of oxygen. If the presence of O^{2-} forces one of the neighboring cerium ions to become Ce^{4+} for charge compensation, a bulky quenching center is created, since intervalence charge-transfer transitions (Sect. 2.3.7) are at low energy and yield seldom emission [39]. If we add to this loss the Auger process mentioned above, it is understandable that the light yield of CeF_3 is considerably lower than is expected.

Moses et al. [36] have determined the quantum efficiency (Sect. 4.3) of the CeF_3 luminescence. For direct Ce^{3+} excitation it is high. Lower quantum efficiencies are found if the excitation starts at the F^- ion ($2p$). For 100 eV the total quantum efficiency is about 0.7. The energy efficiency is then 3%. Also this is relatively low, and the authors suggest nonradiative recombination on quenching centers in order to explain this.

9.5.6 Other Ce^{3+} Scintillators and Related Materials

The strong potential of scintillators like $Gd_2SiO_5:Ce^{3+}$, $Lu_2SiO_5:Ce^{3+}$ and CeF_3 have prompted a search for other Ce^{3+}-activated scintillators. Recently many new ones have been proposed [1,9,11]. Some of these have been included in Table 9.7. New ones are still appearing.

Here we mention $BaF_2:Ce^{3+}$, $YAlO_3:Ce^{3+}$ and $Y_3Al_5O_{12}:Ce^{3+}$ (see Table 9.7). Further there are reports on CeP_5O_{14} ($\tau \sim 30$ ns, light yield 4000 photons MeV^{-1} [11]), $LuPO_4:Ce^{3+}$ (25, 17200 [11]), $CsGd_2F_7:Ce^{3+}$ (30, 10000 [40]), and $GdAlO_3:Ce^{3+}$ ($\tau \sim 1$ ns, which is very short; no light yield given [41]).

A slightly different approach is the use of Nd^{3+} as suggested by Van Eijk's group [9]. The Nd^{3+} ion has $4f^3$ configuration with a $5d \rightarrow 4f$ emission transition in the ultraviolet ($\sim$ 175 nm). Since this is an allowed transition at very high energy, the radiative decay time is even shorter than for Ce^{3+}, viz. 6 ns (in $LaF_3:Nd^{3+}$). See also Sect. 3.3.3. The light yield is a few hundred photons per MeV. Several other host lattices have been tried, but light yields never surpass 1000 photons MeV^{-1} [42]. An important problem is formed by the absorption of Nd^{3+} emission by rare earth impurities.

9.5.7 BaF_2 (Cross Luminescence; Particle Discrimination)

The optical transitions in the luminescence of BaF_2 are discussed in Sect. 3.3.10. Two emissions are observed, a very fast cross luminescence ($\tau = 0.8$ ns, emission maxima 195 and 220 nm) and a much slower self-trapped exciton emission ($\tau = 600$ ns, maximum $\sim$ 310 nm) which is for the greater part quenched at room temperature.

Table 9.8. Some properties of BaF_2

density	4.88 g cm^{-3}
maximum emission wavelengths	310 nm (slow) 220 and 195 nm (fast)
decay times	630 ns (slow) 0.8 ns (fast)
light yield	6.500 photons MeV^{-1} (slow) 2.500 photons MeV^{-1} (fast)

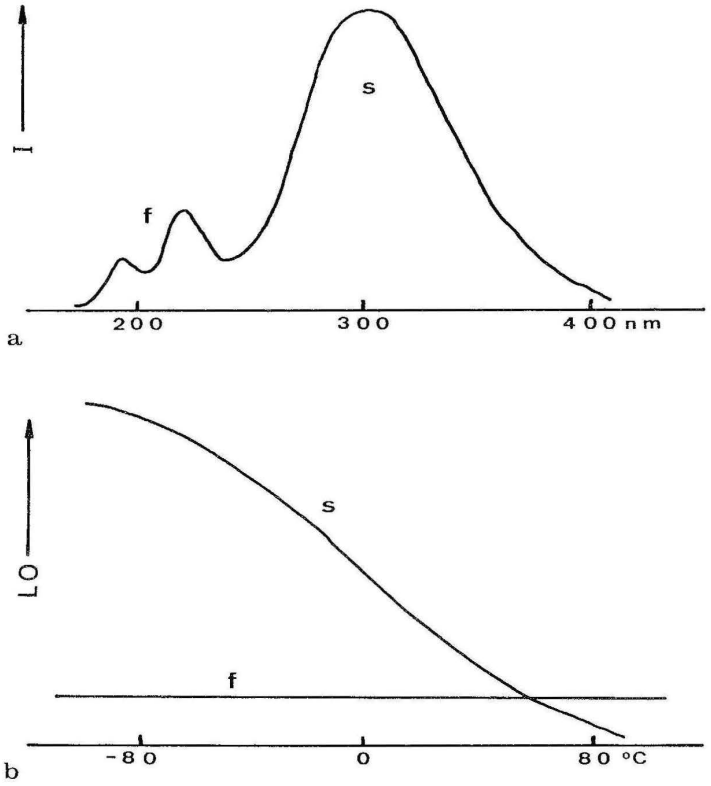

Fig. 9.12. Some data on the scintillation of BaF_2. (*a*): emission spectrum at room temperature under γ-ray excitation; the slow component is indicated by *s*, the fast component by f. (*b*): temperature dependence of the light output (*LO*) of BaF_2 under γ-ray excitation in a wide region around room temperature; the fast component (*f*) is temperature independent, the slow component (*s*) decreases strongly with increasing temperature

BaF_2 is not hygroscopic and large crystals can be grown. The slow emission component can be reduced by a factor of four by adding 1% LaF_3. Table 9.8 gives some of its properties, whereas Fig. 9.12 shows the emission spectrum and the temperature dependence of both components [26].

At the moment there is excellent agreement between the observed emission spectrum of BaF_2 and the spectrum obtained from an ab initio calculation on basis of a molecular cluster approach [43,44]. This confirms the spectral assignments. The relatively low light yield of the fast component is a drawback for the application. Unfortunately the slow emission component is also of an intrinsic nature and captures a greater share of the electron-hole pairs than the fast component. The whole topic has been reviewed by Van Eijk [9,45].

The BaF_2 scintillator can be nicely used for particle discrimination (see Sect. 9.3 and Fig. 9.5), because the intensity ratio of the fast and the slow components of the emission depends on the nature of the excitation. Figure 9.5 shows clearly that the heavier the exciting particles are, the less fast emission there is. The literature does not seem to contain an explanation for this effect. It should be realized that heavy particles will not penetrate deeply into the scintillator. This means that the excitation density must be very high. Since at room temperature the exciton will be more mobile than the electron-hole pair responsible for the cross luminescence, Auger interactions (Sects. 4.6 and 9.5.5) will effect the fast component more strongly than the slow component. Note an interesting wordplay here: whereas the excited state of the cross luminescence is fast in the emission process, it is slow as far as migration through the lattice is concerned (the reason for this is the strongly localized character of the hole in the Ba $5p$ core band; see Fig. 3.27). The slowly emitting exciton is fast in the lattice.

9.5.8 Other Materials with Cross Luminescence

In view of the strong interest in very fast scintillator emission, it is not surprising that many other compounds have been investigated for cross luminescence. It is essential, of course, that the cross-luminescence emission energy is smaller than the bandgap energy, since otherwise the cross luminescence cannot be emitted (see also Fig. 3.27). This is illustrated in Table 9.9 [9]. The table shows excellent agreement between prediction and observation.

Table 9.10, finally, shows some compounds for which cross luminescence has been definitely observed [9]. All decay times are of the same order of magnitude ($\sim$ 1 ns), whereas the light yields do not reach the level of 2000 photons MeV^{-1}. It is, at this time, too early to predict whether cross luminescence will have an important application or not.

9.6 Outlook

For many years scintillator research was often performed in the conviction that the physical mechanisms were unknown, that predictions were impossible, and that new materials should be found by trial and error [46]. As shown in this book and elsewhere

Table 9.9 On the possibility of cross luminescence [9]

compound	E_c–E_{VB}[a] (eV)	E_g[b] (eV)	predicted[c]	observed[d]
BaF_2	4.4–7.8	10.5	+	+
SrF_2	8.4–12.8	11.1	o	–/STE
CaF_2	12.5–17.3	12.6	–	–/STE
CsCl	1–5	8.3	+	+
CsBr	4–6	7.3	+	+
CsI	0–7	6.2	0	–/STE
KF	7.5–10.5	10.7	+	+
KCl	10–13	8.4	–	–/STE

a energy differences between top of core band and bottom or top of the valence band
b energy gap
c +: cross luminescence (CL) possible, –: CL impossible, o: CL doubtful
d +: CL observed, –: no CL observed, STE: exciton emission observed

Table 9.10. Scintillators with cross luminescence at 300 K [9]

compound	emission maximum (nm)	light yield (photons MeV^{-1})	τ (ns)
BaF_2	195, 220	1400	0.8
CsF	390	1400	2.9
CsCl	240, 270	900	0.9
RbF	203, 234	1700	1.3
$KMgF_3$	140–190	1400	1.5
$KCaF_3$	140–190	1400	< 2
KYF_4	140–190	1000	1.9
$LiBaF_3$	230	1400	1
$CsCaCl_3$	250, 305	1400	< 1

[10,11,47], such a conviction is not justified. The knowledge from other fields of luminescence can be very helpful. The light yield is predictable from Eq. (4.6); η_{max} is a well-known quantity in cathodoluminescence and q in photoluminescence. The transfer factor S in Eq. (4.6) is hard to predict and depends probably on the perfection and purity of the crystals. Decay times are easily predictable (see Sect. 3.3).

Modern instrumentation, in addition, offers large potential in studying fundamental processes in scintillators. In the first place the synchrotron should be mentioned which makes monochromatic excitation up to very high energies possible. Examples were mentioned above [36,37].

These developments tend to promote scintillator research into becoming "big science". Also, international cooperation is increasing (see, for example, Ref. [38]), and the multidisciplinarity of this type of research is growing. Actually, the short history of the CeF_3 scintillator sketched above illustrates all these developments very well.

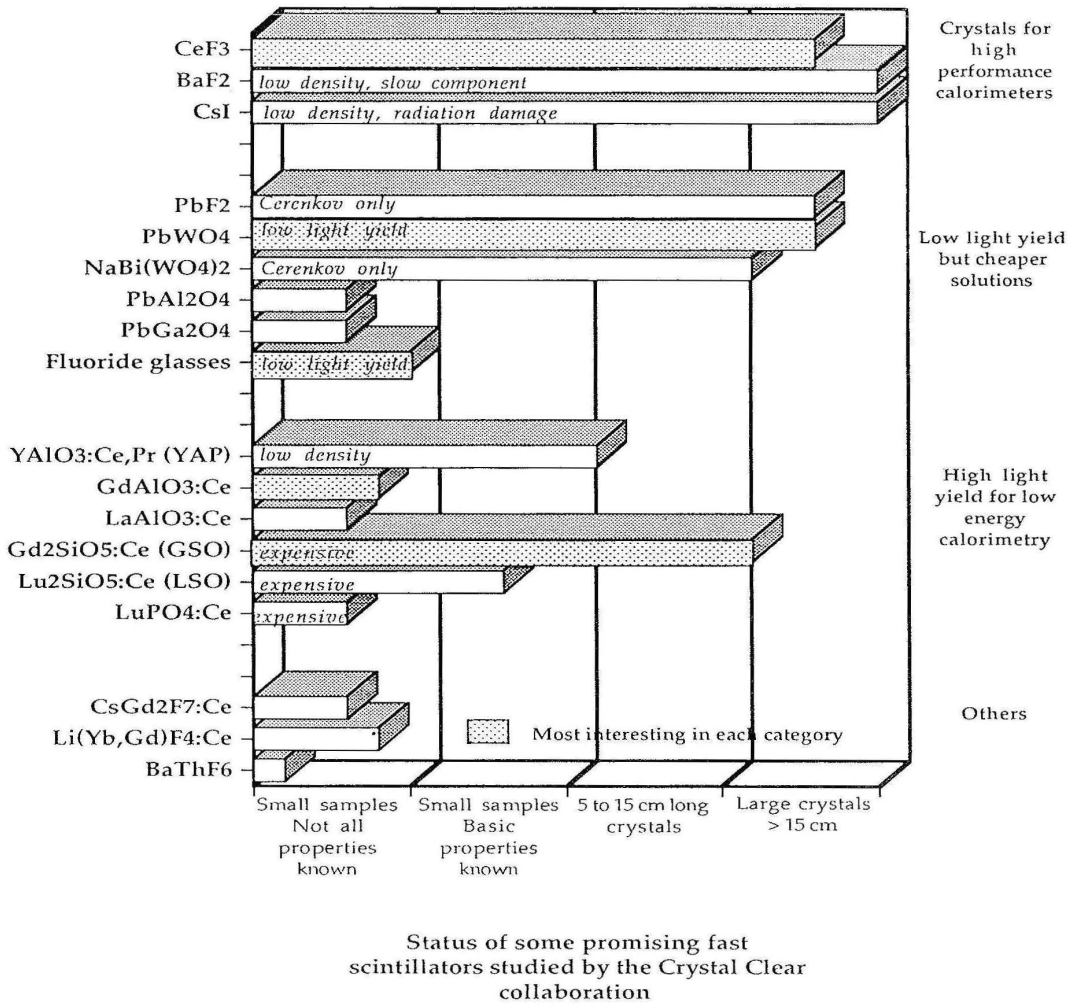

Fig. 9.13. An overview of scintillator research in the Crystal Clear collaboration on scintillator crystals for calorimeter application (1993). Reprinted with permission from their status report of 3rd September 1993

This does not necessarily mean that many new scintillators can be expected. The reason for this view is in the transfer factor S. In order to bring it close to 1, it is necessary to work with simple systems, and many of these have already been checked. For the same reason we do not have high expectations of amorphous scintillators. They contain "intrinsically" too many centers which will contribute to quenching. The open areas will soon be filled in using the theory available at the moment. However, to optimize a given composition to a scintillator which satisfies the requirements of the application is still a hell of a job. It requires cooperation between materials scientists of several backgrounds (crystal growth, defect chemistry, solid state physics, materials science, spectroscopy, and radiation damage). An example of such a group is the

Crystal Clear Collaboration (see authors of Ref. [38]). Figure 9.13 illustrates results from their work as summarized in the Status Report of this group of 3 September 1993. It will be interesting to see how this picture evolves in the coming years.

References

1. De Notaristefani F, Lecoq P, Schneegans M (1993) (eds), Heavy scintillators for scientific and industrial applications. Editions Frontieres, Gif-sur-Yvette
2. Lecoq P (1994) J Luminescence 60/61:948
3. Knoll GF (1987) Radiation detection and measurement, Wiley, New York
4. Grabmaier BC, p 65 in Ref. [1]; J Luminescence 60/61:967
5. Schotanus P (1988) thesis, Technical University, Delft
6. Anderson DF (1982) Phys Letters B118:230
7. Melcher CL, p 75 in Ref. [1]
8. van Eijk CWE, pp 161 and 601 in Ref. [1]
9. van Eijk CWE (1993) Nucl. Tracks Radiat. Meas. 21:5
10. Blasse G (1994) J Luminescence 60/61:930
11. Lempicki A, Wojtowicz AJ (1994) J Luminescence 60/61:942; Lempicki A, Wojtowicz AJ, Berman E (1993) Nucl Instr Methods A322:304
12. McKeever SWS (1985) Thermoluminescence of solids, Cambridge University, Cambridge; McKeever SWS, Markey BG, Lewandowski AC (1993) Nucl. Tracks Radiat. Meas. 21:57
13. Azorin J, Furetta C, Scacco A (1993) Phys Stat Sol(a) 138:9
14. Wisshak K, Guber K, Kappeler F, Krisch J, Müller H, Rupp G, Voss F (1990) Nucl. Instr. Methods A292:595
15. Migneco E, Agodi C, Alba R, Bellin G, Coniglione R, Del Zoppo A, Finocchiaro P, Maiolino C, Piattelli P, Raia G, Sapienza P (1992) Nucl. Instr. Methods A 314:31
16. Nestor OH (1983) Mat. Res. Soc. Symp. Proc. 16:77
17. Grabmaier BC (1984) IEEE Trans. Nucl. Sci. NS-31:372
18. Takagi K, Fukazawa T (1983) Appl. Phys. Lett. 42:43
19. Goriletsky VI, Nemenov VA, Protsenko VG, Radkevich AV, Eidelman LG (1980) Proc. 6th conf. on crystal growth, Moscow, p III 20
20. Chongfau H (1987) (Shanghai Institute of Ceramics, Academia Sinica, unpublished manuscript), cited as ref. 59 by Gévay G, Progress Crystal Growth Charact 15:181
21. Wilke KTh, Bohm J (1988) Kristallzüchtung. Verlag Harry Deutsch, Thun (in German)
22. Anthony AM, Collongues R (1972) In: Hagenmuller P (ed) Preparative methods in solid state chemistry. Academic, New York, p 147
23. West AR (1984) Solid state chemistry and its applications. Wiley, New York, Sect. 2.7
24. Ishii M, Kobayashi M (1991) Progress Crystal Growth Charact 23:245
25. Gévay G (1987) Progress Crystal Growth Charact 15:145
26. Schotanus P (1992) Scintillation Detectors, Saint-Gobain, Nemours
27. Weber MJ (1987) Ionizing Radiation (Japan) 14:3
28. Grabmaier BC, Haussühl S, Klüfers P (1979) Z. Krist. 149:261
29. Timmermans CWM, Boen Ho O, Blasse G (1982) Solid State Comm 42:505
30. Timmermans CWM, Blasse G (1984) J Solid State Chem 52:222
31. Blasse G (1968) Philips Res Repts 23:344
32. Ishii M, Kobayashi M, Yamaga I, p 427 in Ref. [1]
33. Suzuki H, Tombrello TA, Melcher CL, Schweitzer JS (1992) Nucl. Instrum. Methods A 320:263
34. Lammers MJJ, Blasse G (1987) J. Electrochem. Soc. 134:2068; unpublished measurements
35. Dirksen GJ, Blasse G (1993) J. Alloys Compounds 191:121
36. Moses WW, Derenzo SE, Weber MJ, Cerrina F, Ray-Chaudhuri A (1994) J Luminescence 59:89

37. Pedrini C, Moine M, Boutet D, Belsky AN, Mikhailin VV, Viselev AN, Zinin EI (1993) Chem Phys Letters 206:470
38. Anderson S, Auffray E, Aziz T, Baccaro S, Banerjee S, Bareyre P, Barone LE, Borgia B, Boutet D, Burg JP, Chemarin M, Chipaux R, Dafinei I, D'Atonasio P, De Notaristefani F, Dezillie B, Dujardin C, Dutta S, Faure JL, Fay J, Ferrère D, Francescangeli OP, Fuchs BA, Ganguli SN, Gillespie G, Goyot M, Gupta SK, Gurtu A, Heck J, Hervé A, Hillimanns H, Holdener F, Ille B, Jönsson L, Kierstead J, Krenz W, Kway W, Le Goff JM, Lebeau M, Lebrun P, Lecoq P, Lemoigne Y, Loomis G, Lubelsmeyer K, Madjar N, Majni G, El Mamouni H, Mangla S, Mares JA, Martin JP, Mattioli M, Mauger GJ, Mazumdar K, Mengucci PF, Merlo JP, Moine B, Nikl N, Pansart JP, Pedrini C, Poinsignon J, Polak K, Raghavan R, Rebourgeard P, Rinaldi DT, Rosa J, Rosowsky A, Sahuc P, Samsonov V, Sarkar S,Schegelski V, Schmitz D, Schneegans M, Seliverstov D, Stoll S, Sudhakar K, Svensson A, Tonwar SC, Topa V, Vialle JP, Vivargent M, Wallraff W, Weber MJ, Winter N, Woody C, Wuest CR, Yanovski V (1993) Nucl. Instrum. Methods A332:373
39. Blasse G (1991) Structure and Bonding 76:153
40. Dorenbos P, Visser R, van Eijk CWE, Khaidukov NM, p 355 in Ref. [1]
41. Mares JA, Pedrini C, Moine B, Blazek K, Kvapil J (1993) Chem Phys Letters 206:9
42. Visser R, Dorenbos P, van Eijk CWE, p 421 in Ref. [1]
43. Andriessen J, Dorenbos P, van Eijk CWE (1991) Molec. Phys. 74:535
44. Andriessen J, Dorenbos P, van Eijk CWE (1993) Nucl. Tracks Radiat. Meas. 21:139
45. van Eijk CWE (1994) J Luminescence 60/61:936
46. Blasse G (1991) IEEE Trans. Nucl. Science 38:30 47. Blasse G, p 85 in Ref. [1]

CHAPTER 10

Other Applications

Luminescence has lead to many more applications than those discussed in the previous four chapters. In this chapter some of these will be discussed shortly. For this purpose we selected the following topics: upconversion, the luminescent center as a probe, luminescence immuno-assay, electroluminescence, optical fibers, and small particles.

10.1 Upconversion: Processes and Materials

10.1.1 Upconversion Processes

The principle of upconversion is schematically given in Fig. 10.1. This figure shows the energy level structure of an ion with ground state A and excited levels B and C. The energy differences between levels C and B and levels B and A are equal. Excitation

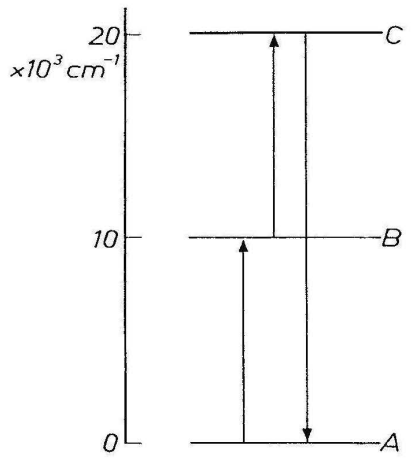

Fig. 10.1. The principle of upconversion. The infrared excitation radiation (10 000 cm^{-1}) is converted into green emission (20 000 cm^{-1})

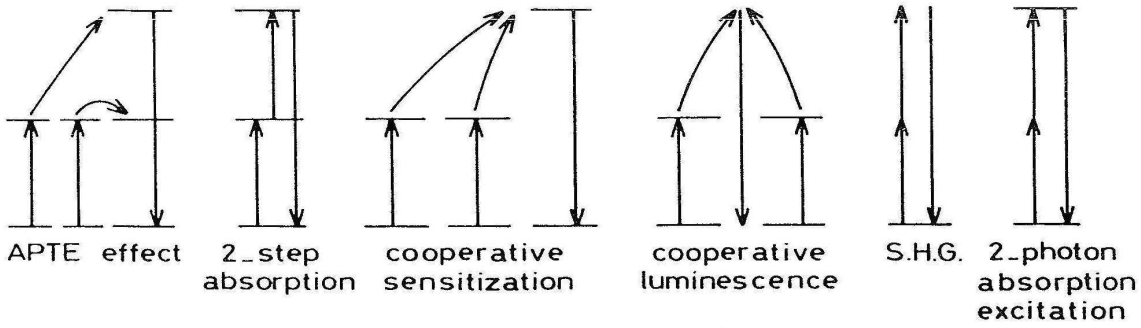

Fig. 10.2. The several upconversion processes according to Auzel [1]. See also text

occurs with radiation the energy of which corresponds to this energy difference, so that the ion is excited from A to B. If the life time of level B is not too short, the excitation radiation will excite this ion further from B to C. Finally emission from C to A may occur. Let us assume that the energy difference B-A and C-B is 10 000 cm^{-1} (corresponding to infrared excitation), then the emission is at 20 000 cm^{-1}, i.e. in the green. This is really anti-Stokes emission! It will also be clear that in this way we can detect infrared radiation visually. After this oversimplified introduction we now turn to a more serious consideration. Here we follow a treatment given by Auzel [1].

Actually there are many upconversion processes possible with widely different conversion efficiencies. Their energy schemes are given in Fig. 10.2. From left to right the following processes are shown:

- upconversion by energy transfer (Chapter 5), sometimes called the APTE effect (Addition de Photons par Transfers d'Energie). Here ions A transfer subsequently their excitation energy to another ion B which can now emit from a higher level.
- upconversion by two-step absorption (the example of Fig. 10.1) which needs only the B ion.
- upconversion by cooperative sensitisation: two ions A transfer simultaneously their excitation energy to ion C which has no energy level at the position of the excited level of A. Emission occurs from the excited level of C.
- cooperative luminescence: two A ions combine their excitation energy to one quantum which is emitted (note, however, that there is no real emitting level).
- second harmonic generation (frequency doubling) in which the frequency of the irradiated light is doubled (without any absorption transition taking place).
- two-photon absorption in which two photons are simultaneously absorbed without using any real intermediary energy level at all. The emission occurs by one photon from the excited energy level.

Table 10.1 gives some idea of the efficiency of the upconversion processes [2]; the efficiencies given relate to normalized incident power (1 W cm^{-2}). Also some examples of systems which show the relevant process are given. Table 10.1 together with Fig. 10.2 show that the higher-efficient processes require energy levels which are resonant with the incoming or outgoing radiation. This is not the case for the latter three, which will not be considered further.

Table 10.1 The different two-photon upconversion processes, their mechanism, their efficiency normalized to incident power (1 W cm^{-2}), and an example, after Refs [1] and [2]. Compare Fig. 10.2

Mechanism	Efficiency	Example
Sequential energy transfer (APTE)	10^{-3}	$YF_3 : Yb^{3+}, Er^{3+}$
Two-step absorption	10^{-5}	$SrF_2 : Er^{3+}$
Cooperative sensitization	10^{-6}	$YF_3 : Yb^{3+}, Tb^{3+}$
Cooperative luminescence	10^{-8}	$YbPO_4$
Second harmonic generation	10^{-11}	KH_2PO_4
Two-photon excitation	10^{-13}	$CaF_2 : Eu^{2+}$

10.1.2 Upconversion Materials

a. Materials with Yb^{3+} and Er^{3+}

The first example of upconversion was reported in 1966 by Auzel for the couple Yb^{3+}, Er^{3+} in $CaWO_4$ [3]. Figure 10.3 shows the energy level schemes involved. Near-infrared radiation (970 nm) is absorbed by Yb^{3+} ($^2F_{7/2} \rightarrow {}^2F_{5/2}$) and transferred to Er^{3+}, so that the $^4I_{11/2}$ level of Er^{3+} is populated. During the lifetime of the $^4I_{11/2}$ level a second photon is absorbed by Yb^{3+} and the energy transferred to Er^{3+}. The Er^{3+} ion is now raised from the $^4I_{11/2}$ to the $^4F_{7/2}$ level. From here it decays rapidly and nonradiatively to the $^4S_{3/2}$ level from which a green emission occurs ($^4S_{3/2} \rightarrow {}^4I_{15/2}$). In this way green emission is obtained from near-infrared excitation.

Since two infrared quanta are required to produce one green quantum, the emission intensity will increase quadratically with the density of the infrared excitation. This has been observed, and is proof of the two-photon character of the excitation. Efficiencies are therefore only useful if the excitation density is given.

In Table 10.2 the efficiency of the green emission intensity of Yb^{3+}, Er^{3+}-codoped host lattices under infrared excitation is given [4]. The excitation density is the same, as are the activator concentrations. It is seen that the efficiency depends strongly on the choice of the host lattice. That of α-$NaYF_4$ yields very efficient upconversion materials [5]. Oxides are less suitable than fluorides, since lifetimes in oxides are shorter than in fluorides due to a stronger interaction between the luminescent ion and its surroundings (Sect. 2.2). If the lifetime of the intermediary $^4I_{11/2}$ level is decreased, the total efficiency of the upconversion process will also decrease.

These materials are therefore able to convert infrared into green light. As an example, a GaAs diode (see Sect. 10.4) which yields infrared emission can be covered with a Yb^{3+}, Er^{3+}-codoped fluoride layer and yield green emission. However, there is no real advantage in this system, since a GaP diode yields green light directly. Although the efficiency of the GaAs diode is higher, the efficiency of the upconversion process is so low that the combination cannot really compete with the single GaP diode.

b. Materials with Yb^{3+} and Tm^{3+}

Figure 10.4 shows the relevant energy levels. Infrared radiation can be converted into

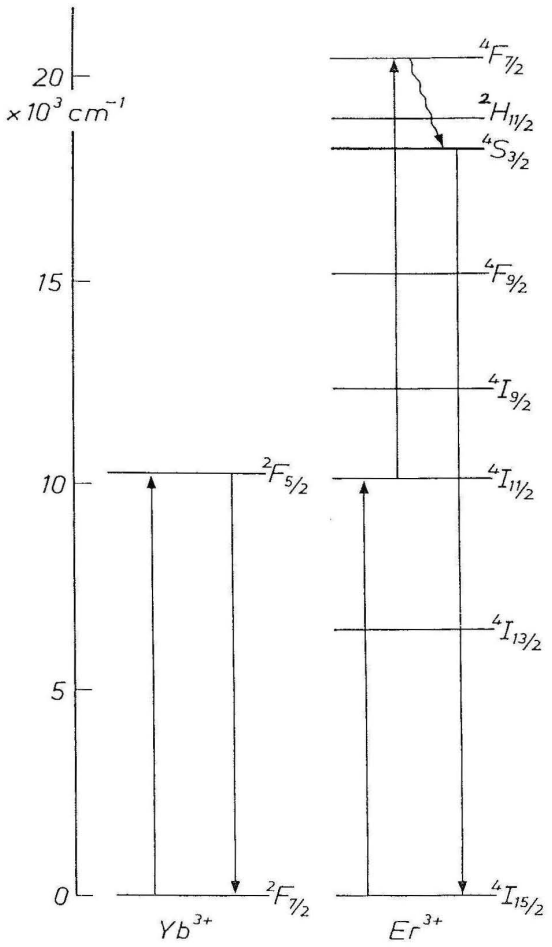

Fig. 10.3. Upconversion in the Yb^{3+}, Er^{3+} couple. Exciton is into Yb^{3+}, emission from the $^4S_{3/2}$ level of Er^{3+}

blue emission by a three-photon upconversion process. After one transfer step the $^3H_5$ level of Tm^{3+} is populated. This decays rapidly to the $^3F_4$ level. The second transfer step raises the Tm^{3+} ion from $^3F_4$ to $^3F_2$ which decays to $^3H_4$. Subsequently the third transfer step raises the Tm^{3+} ion from $^3H_4$ to $^1G_4$ which yields a blue emission. Its intensity increases linearly with the third power of the excitation density.

For Er^{3+} Auzel has described upconversion processes using summations of up to five photons [1]. In this way 970 nm radiation is converted into 410 nm radiation. Several of the transfer steps are not resonant, so that energy is lost to phonons in the transfer process. The first transfer step in the couple Yb^{3+}, Tm^{3+} is an illustrative example (see Fig. 10.4).

c. Materials with either Er^{3+} or Tm^{3+}

From Sect. 10.1.1 it is clear that materials doped with only one ion can only show

Table 10.2 Normalized green emission intensity under infrared excitation of Yb^{3+}, Er^{3+}-codoped host lattices [4]

Host lattice	Intensity
α-$NaYF_4$	100
YF_3	60
$BaYF_5$	50
$NaLaF_4$	40
LaF_3	30
La_2MoO_8	15
$LaNbO_4$	10
$NaGdO_2$	5
La_2O_3	5
$NaYW_2O_6$	5

upconversion with reasonable efficiency by the two- or more-step photon absorption process (Fig. 10.1). Two examples are given in Fig. 10.5. On the left-hand side the Er^{3+} ion converts 800 nm radiation into 540 nm radiation, on the right-hand side the Tm^{3+} ion converts 650 nm radiation into 450 and 470 nm radiation.

For application (see below) the ions are irradiated with a laser diode (Sect. 10.4): Er^{3+} absorbs 800 nm from an AlGaAs laser diode, Tm^{3+} absorbs 650 nm from newly developped laser diodes. Figure 10.5 shows that the Er^{3+} ion reaches the green-emitting $^4S_{3/2}$ level by subsequently absorbing two photons. Two different pathways are indicated; their relative importance depends on the ratio of the different transition rates. Also the Tm^{3+} ion reaches the blue emitting $^1D_2$ and $^1G_4$ levels by a two-step process. In both cases a quadratic dependence of emission intensity upon excitation power has been observed [6].

In fluoride glasses, these ions show a high upconversion efficiency, in contrast to silicate glasses (see also Sect. 10.1.2.a). A suitable glass is ZBLAN ($53ZrF_4$, $20BaF_2$, $4LaF_3$, $3AlF_3$, 20NaF). Figure 10.6 gives the upconversion emission of ZBLAN glass with Er^{3+} under 800 nm irradiation. The $^2G_{9/2} \rightarrow {}^4I_{15/2}$ emission is very weak because of the fast nonradiative decay from $^2G_{9/2}$ to lower levels (see Fig. 10.5). The weak $^4F_{9/2} \rightarrow {}^4I_{15/2}$ emission is due to a small amount of nonradiative decay from $^4S_{3/2}$ to $^4F_{9/2}$.

The potential application of this glass is in high-density optical recording (used, for example, in compact disc players). In such devices the information density increases with decreasing size of the focus spot of the laser. This size varies inversely quadratically with the wavelength. Since the available diode lasers emit in the near infrared, there is a considerable amount of research going on to obtain a blue-emitting diode laser. There are three possibilities, viz.

(1) the search for a blue-emitting laser diode which does not exist at the moment, but may be developed on the basis of zinc sulfide. The realization of such a laser seems to be near.

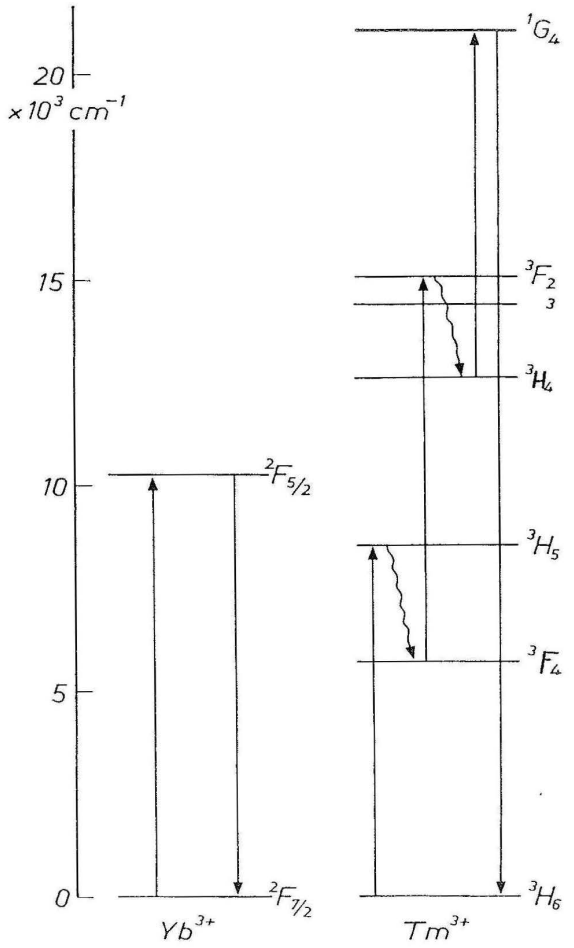

Fig. 10.4. Upconversion in the Yb^{3+}, Tm^{3+} couple. The emitting $^1G_4$ level of Tm^{3+} is reached after three successive energy transfer steps from Yb^{3+}

(2) frequency-doubling of the near-infrared laser radiation by second harmonic generation (see Fig. 10.2); materials for this purpose are $KNbO_3$ and $K_3Li_{1.97}Nb_{5.03}O_{15.06}$ [7].
(3) based upon the above-mentioned two-step absorption processes a fluoride-glass fiber can be made which acts as an upconversion laser, pumped by a laser diode.

d. Concluding Remarks

The materials mentioned above show that especially the trivalent rare earth ions are very suitable for upconversion processes. This is not surprising in view of their energy level schemes (see Fig. 2.14). These show often a wealth of intermediary levels. Upconversion has, however, also been observed for other ions. Examples are $5f^n$ ions (U^{4+} and Np^{4+} in $ThBr_4$ [8]), and transition metal ions ($MgF_2 : Ni^{2+}$).

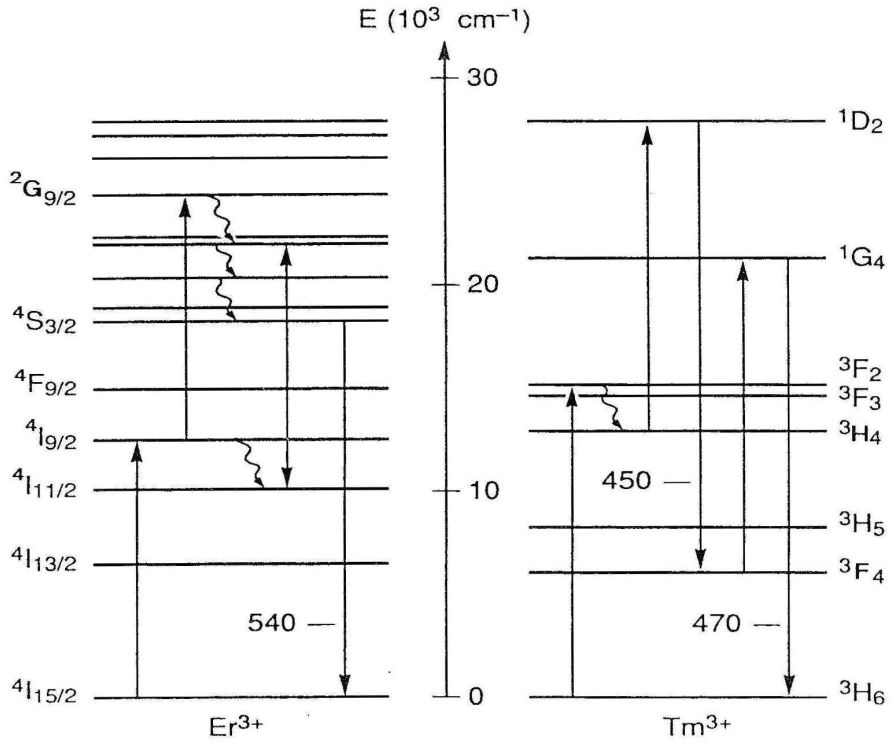

Fig. 10.5. Upconversion in one ion, illustrated on Er^{3+} and Tm^{3+}

The positive role of upconversion in the field of materials has already been outlined above. There are also negative aspects of upconversion, viz. saturation effects. This is due to the fact that upconversion implies a transition from an excited state upwards. If we are interested in the emission from this specific excited state, either in view of its luminescence or its stimulated emission, we have to consider the fact that upconversion will decrease the population of this level, so that the intensity of the emission of interest decreases. This will especially be the case for higher activator concentrations and/or high excitation densities (saturation effect).

Part of the saturation effects in projection-television phosphors (see Sect. 7.3.4) can be ascribed to an upconversion process of the type shown in Fig. 10.7. This is very similar to the Auger processes mentioned for semiconductors (see Sect. 4.6). Often this type of upconversion prevents a material from becoming a good laser material. If the stimulated emission radiation is reabsorbed by ions which are still in the excited state, the laser efficiency drops. From Fig. 10.7, it becomes clear that the upconversion process, which is, in this case, usually called excited state absorption, influences the population inversion in a negative way: considering the two ions in Fig. 10.7, the population inversion is complete before the upconversion occurs, but after upconversion and nonradiative decay to the emitting state, the population

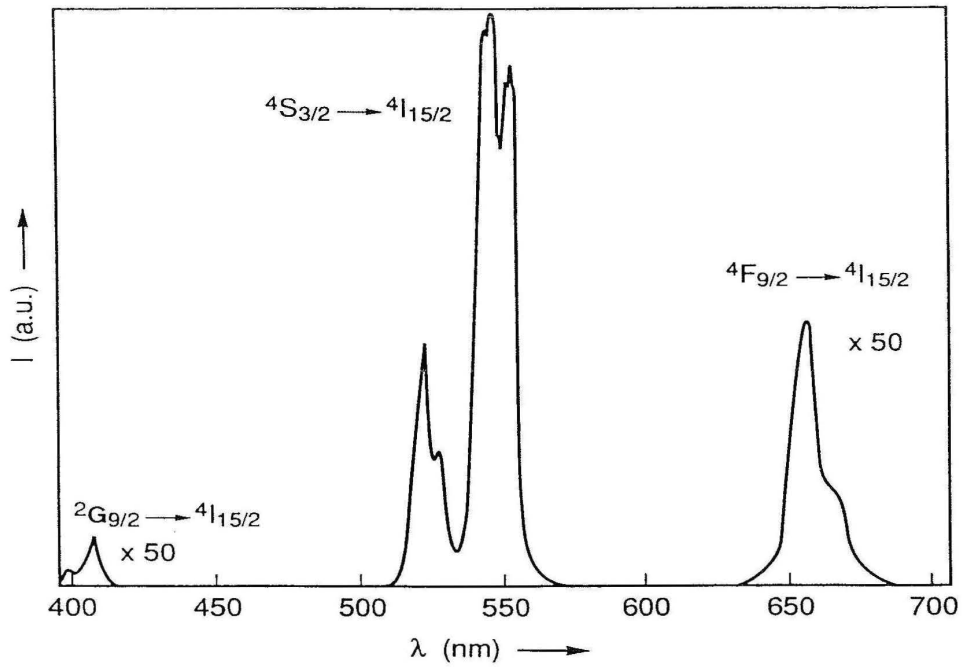

Fig. 10.6. The emission spectrum of Er^{3+}-doped ZBLAN glass in the visible spectral region under infrared excitation. Reproduced with permission from Ref. [6]

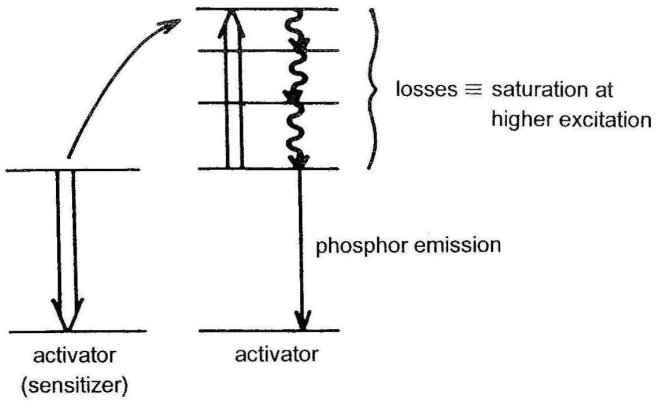

Fig. 10.7. Upconversion as a quenching process of the luminescence in a phosphor

inversion has decreased to 50%. For this reason excited-state absorption studies are popular among those who investigate potential laser materials.

For recent developments the reader is referred to the Proceedings of the International Conference in Luminescence 1993 (J. Luminescence, (1994) 60/61).

10.2 The Luminescent Ion as a Probe

The use of luminescent ions as a probe does not belong to the field of industrial application of luminescent materials, but should be considered as an application in the field of research and characterisation of materials. The basic idea is that the luminescence properties of an ion tell us something about the ion itself and also about its surroundings in the host lattice. The dangerous side of this use of luminescence, a side which is often overlooked, is that only luminescent ions can be monitored. However, it may well be that the material contains the specific ion but that it does not or only partly luminesce under the given circumstances. It is therefore important to know whether the ion has really been excited or not, and whether all ions show emission or not.

The luminescence of ions can be used as a tool for their chemical analysis. Fassel et al. [9] have described the techniques of optical atomic emission and X-ray excited optical luminescence for chemical analysis of rare earth elements. It is essential that the elements that are to be analysed are excited with high efficiency, and luminesce with high quantum efficiency. Under these circumstances analyses can be made in the ppm region, and sometimes even lower. An illustrative example is $GdAlO_3$ which shows always Cr^{3+} emission upon Gd^{3+} excitation [10]). The excitation energy on the Gd^{3+} ion migrates over the Gd^{3+} sublattice (Sect. 5.3.1) and is captured efficiently by the Cr^{3+} impurities which were present in the starting material containing aluminium. In the same way the rutile modification of TiO_2 shows always Cr^{3+} emission upon excitation into the band-band transition of rutile. The created free charge carriers (Sect. 3.3.9) recombine on the Cr^{3+} impurities and make it very hard to investigate the intrinsic rutile luminescence [11]. These experiments show that aluminium- and titanium compounds often contain some chromium. In addition the excitation routes in $GdAlO_3$ and TiO_2 are very efficient.

How luminescent ions can function as a probe of their surroundings, is easily understood from a consideration of Fig. 3.10. The Eu^{3+} ion shows very different emissions in $NaGdO_2$ and $NaLuO_2$. If the crystal structures were not known, one could find from these spectra that the Na^+ and Ln^{3+} ions (Ln = Gd, Lu) are ordered, and that the Eu^{3+} coordination in $NaLuO_2$ has inversion symmetry and that in $NaGdO_2$ not.

In this connection, it is important to note that luminescence yields structural information of a completely different character from that obtained by diffraction (X-rays, neutrons). The latter detects long-range order, i.e. the total crystal structure. The former yields only information on the surroundings of the luminescent ion, and can therefore probe short-range order.

As an example we mention the scheelites Y_2SiWO_8 and Y_2GeWO_8 [12]. X-ray diffraction does not reveal superstructure reflections due to a crystallographic order on the tetrahedral sites. The luminescence of a small amount of Eu^{3+} in these compounds yields other information. The silicon-containing compound shows sharp emission lines indicating a considerable amount of short-range order; however, the germanium containing compound shows emission lines which are an order of magnitude broader indicating a much lower degree of order (Fig. 10.8).

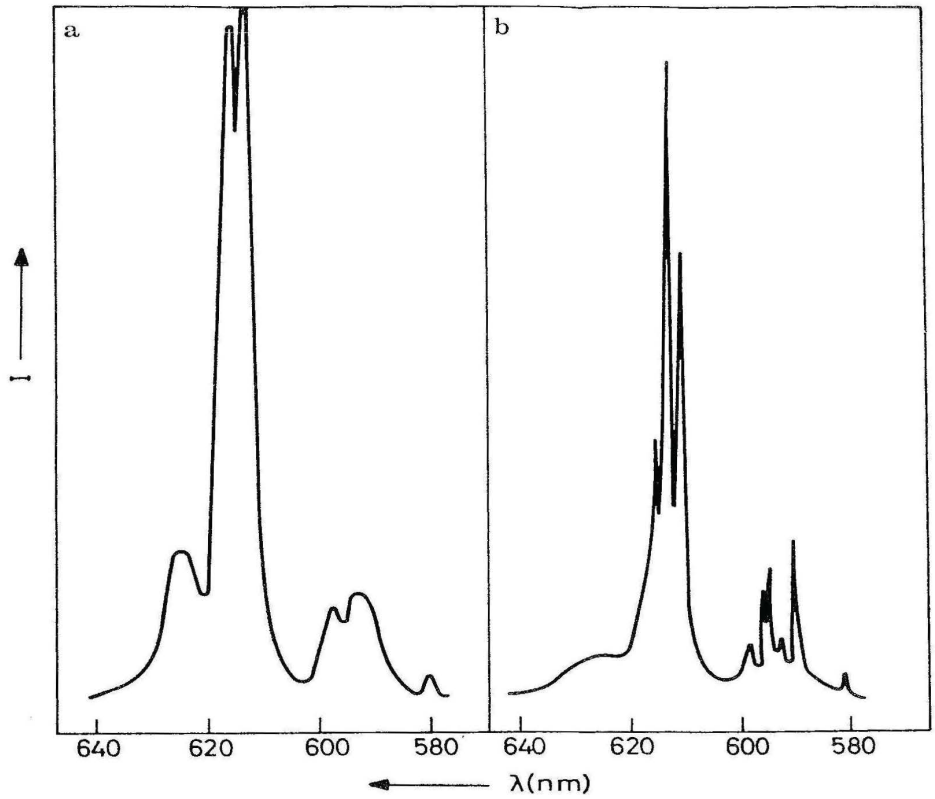

Fig. 10.8. The emission spectra of the Eu^{3+} ion in Y_2GeWO_8 (a) and Y_2SiWO_8 (b)

Often luminescent ions are used to characterise the structure of glasses. In our opinion such measurements yield only information on the surroundings of the luminescent ion in the glass, and not on the glass structure. In addition it should be kept in mind that the luminescent ion, often a network modifier, may locally perturb the glass structure strongly.

Boulon et al. [13,14] used the luminescence of Cr^{3+} in order to investigate the crystallization of a glass and to characterize glass ceramics. Use is made of the fact that the Cr^{3+} ion prefers the crystalline above the amorphous phase. Figure 10.9 shows one of their results. The glass has composition 52% SiO_2, 34.7% Al_2O_3, 12.5% MgO and 0.8% Cr_2O_3. Curve (a) gives the emission spectrum of the glass. It is due to Cr^{3+} ions. Some of these give ^2E emission (around 692 nm), but most of them $^4T_2$ emission (the band around 850 nm) (see also Sect. 3.3.4a). Curve (c) gives the emission of this glass after 10 min heating at 950°C. This is the temperature where crystallization occurs. Now the ^2E emission dominates and has also become sharper. Analysis shows that this emission is mainly due to Cr^{3+} in $MgAl_{2-x}Cr_xO_4$ crystals with 40 nm diameter. In the crystal the inhomogeneous broadening (Sect. 2.2) is less, so that the ^2E emission sharpens relative to that in the glass. In the spinel structure the crystal field on Cr^{3+} is so large that only ^2E emission occurs. The broad band in

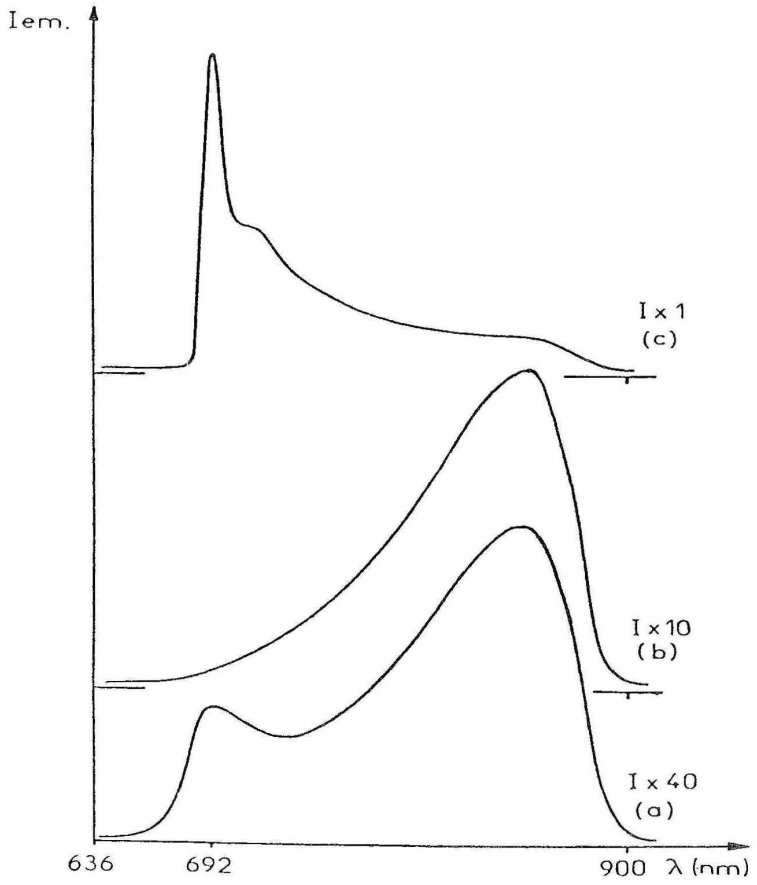

Fig. 10.9. Luminescence spectroscopy of glass crystallization. (a) the Cr^{3+} emission of the glass (^2E and $^4T_2$ emission); (b) the emission of the glass containing $MgCr_2O_4$ crystallites; (c) the emission of the glass containing $MgAl_{2-x}Cr_xO_4$ crystals. Note the large increase in luminescence intensity. See also text. Reproduced with permission from Ref. [13]

curve (c) is due to Cr^{3+} ions which are still in the glass where the crystal field is lower.

Curve (b) is the emission spectrum of a glass annealed at somewhat lower temperature. It has been shown that this glass contains very small $MgCr_2O_4$ crystallites, so that the conclusion follows that the Cr^{3+} ions in the glass cluster together and form $MgCr_2O_4$ crystallites as the very first crystallization step. Later the Cr^{3+} ions are redistributed to form $MgAl_{2-x}Cr_xO_4$, because particle growth occurs by assimilation of Al^{3+} ions.

Phase transitions in crystalline materials have also been followed by luminescence measurements. Examples are the transition crystalline → liquid crystalline in octa-n-dodecoxy substituted phthalocyanine [15] where the luminescence disappears, and the para- to ferroelectric transition in Cr^{3+}-doped $Li_2Ge_7O_{15}$ [16], where the ^2E emission lines are split by the phase transition.

Examples of probing the surroundings are the following:

- in $CaF_2 : Er^{3+}$ the luminescent ion has been found to occupy up to 20 distinct lattice sites [17]. This is due to the fact that the Er^{3+} ion has an excess positive charge relative to Ca^{2+} and requires charge compensation. In the fluorite structure this can occur in many ways, so that many centers appear. This has been found for many trivalent ions in fluorite. Examples of these centers are Er^{3+} without nearby charge compensator, Er^{3+} associated with O^{2-}, with interstitial F^-, associates of Er^{3+} and several F^- ions. By the application of site-selective spectroscopy it is possible to study the thermodynamics of the defect-defect interactions.
- in $CaSO_4$ the Eu^{3+} and other trivalent luminescent ions form associates with V^{5+} : $(Eu^{\bullet}_{Ca}.V'_S)^x$. This follows directly from the emission spectra. Excitation into the vanadate group results in Eu^{3+} emission, because the V-Eu distance is short (nearest neighbors, see Sect. 5.3.2) [18]. Such samples can be considered as solutions of "molecules" $EuVO_4$ into $CaSO_4$. Unfortunately the solubility is low. Otherwise a cheap red-emitting lamp phosphor would have been found (see Sect. 6.5).
- in $CsCdBr_3$ the Cd^{2+} ions form linear chains. If three Cd^{2+} ions are replaced by two Ln^{3+} ions, they form a linear cluster $(Ln^{\bullet}_{Cd} \cdot V''_{Cd} \cdot Ln^{\bullet}_{Cd})^x$. If $Ln = Tb$, such a cluster yields green emission from the $^5D_4$ level because of cross relaxation (Sect. 5.3.1), so that even for low Tb^{3+} concentrations the blue emission intensity is low [19].
- the way in which trivalent lanthanide ions are coordinated on a silica surface can be deduced from their emission spectra [20]. The Ln^{3+} ion is bound directly via Si–O-bonds to the silica and is, on the other side, coordinated by 4 water molecules.
- the way in which the vanadate group is attached to the silica surface in the industrially important catalyst SiO_2–V can be found from luminescence spectroscopy [21]. These materials show a peculiar luminescence: the vanadate emission band shows vibrational structure at low temperature with a spacing between the individual lines of nearly 1000 cm^{-1} (see Fig. 10.10). This indicates the presence of a very short V-O bond. The decay time is very long. All this shows that the V^{5+} ion is bonded to the silica surface with three Si–O–V bonds, whereas one very short V–O bond sticks out of the surface (V–O distance $\sim$ 1.56 Å). It is this V–O bond which is involved in catalytic processes (Fig. 10.11).

10.3 Luminescence Immuno-Assay

10.3.1 Principle

The luminescence of rare earth complexes can be applied in immunology, which is a method for determining biological species, especially for clinical applications. The method is superior to many other methods as far as sensitivity and specificity

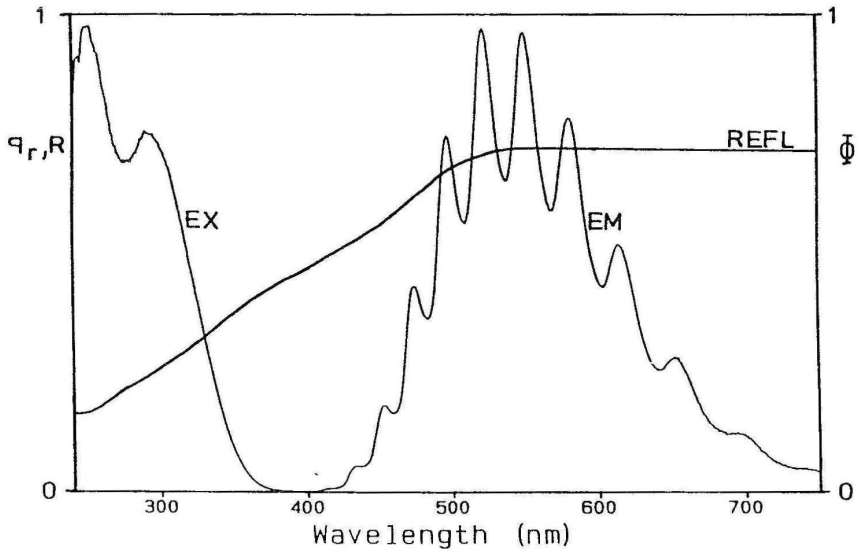

Fig. 10.10. The spectroscopy of SiO_2–V^{5+}. REFL: diffuse reflection spectrum; EX: excitation spectrum of the luminescence; EM: emission spectrum at low temperatures showing vibrational structure. After M.F. Hazenkamp, thesis, University Utrecht, 1992

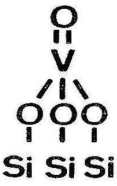

Fig. 10.11. The vanadate group on the silica surface

are concerned. Although this book deals with solid materials only, this application is mentioned here in view of the interesting aspects of the luminescent species involved. Their properties have also a strong analogy to those of luminescent ions in solids. The whole topic has recently been reviewed by Sabbatini et al. [22].

The immunological method based on the use of luminescent labels is usually called fluoroimmunoassay [23]. Here we use the term luminescence immunoassay for the same reasons given in Sect. 6.2 for luminescent lighting. The luminescent label is coupled chemically to an antibody which binds in a specific way to a given biomolecule or organism. In this way the presence of luminescence can be related to the presence of certain molecules or organisms.

Usually the samples have their own luminescence. Therefore rare-earth labels are used. The background luminescence of biological materials is usually short-lived, whereas ions like Eu^{3+} and Tb^{3+} have emitting states with long lifetimes (Sect. 3.3.2.). Therefore these two types of emission can be easily separated.

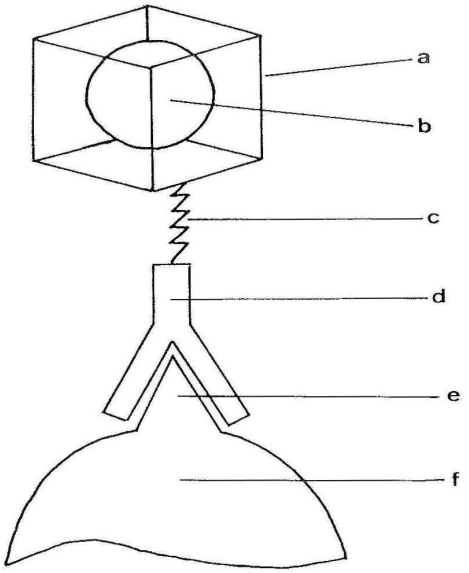

Fig. 10.12. Schematic representation of luminescence immunoassay with a rare-earth cryptate. a: cryptand; b: luminescent rare earth ion; c: connection to antibody; d: antibody; e: antigene; f: biomolecule

Since the whole determination is carried out in aqueous media, the rare-earth ion has to be shielded from its direct environment, because otherwise its luminescence is strongly quenched by the water molecules (Sect. 4.2.1). There are several ways of preventing this, as will be discussed below. In all of these a cage is built around the luminescent ion. Figure 10.12 shows the principle of luminescence immunoassay in a schematic way.

10.3.2 Materials

The commercial kits presently available make use of Eu^{3+} chelates. It is a complicated procedure, since two different chelates are used. More promising are complexes consisting of a rare earth ion and an encapsulating ligand. Several types of these ligands have been proposed, see Ref. [22]. Here we restrict ourselves to the cryptands. A cryptand is a ligand which forms a cage around a metal ion; the whole complex is called a cryptate. An example of such a cryptand is given in Fig. 10.13. The $(Eu \subset 2.2.1)^{3+}$ and $(Tb \subset 2.2.1)^{3+}$ cryptates ($\subset$ stands for encapsulation) show luminescence in aqueous solution, but their quantum efficiencies are low, especially in the case of the Eu^{3+} ion (excitation in the charge-transfer and $4f$-$5d$transition, respectively). The nonradiative losses are due to multiphonon emission involving the water molecules and, in the case of Eu^{3+}, the low energy position of the charge-transfer state (Sect. 4.2.2).

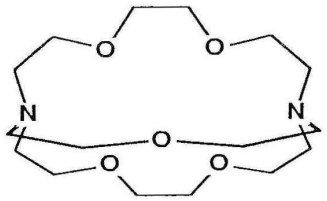

Fig. 10.13. 2.2.1 cryptand

Nevertheless the cryptand shields the rare earth ion from the aqueous medium, since the free rare earth ions have still lower efficiencies in aqueous solution. In the latter case 9 to 10 water molecules coordinate the rare earth ion, whereas in the 2.2.1 cryptate only 3 water molecules are still able to interact with the rare earth ion.

Considerable improvements have been obtained by using cryptands containing organic groups with strong ultraviolet absorption. The prototype is the bpy.bpy.bpy cryptand (bpy = 2,2′-bipyridine). Fig. 1.9 shows the relevant cryptate. This cryptate shows a high output of the lanthanide emission, because ultraviolet radiation is strongly absorbed in the bpy groups. The absorbed energy is subsequently transferred to the rare earth ion, from where emission occurs. There is a strong analogy with $YVO_4 : Eu^{3+}$ (Sect. 5.3.2). The VO_4^{3-} group as well as the bpy complex are efficient sensitizers (Sect. 5.1) of the rare earth emission. In the language of photochemists this is called the antenna effect [22].

However, nonradiative losses also occur here, because the cryptand does not shield the rare earth ion completely. Even for Tb^{3+} the quantum efficiency is low. This is due to the presence of a charge-transfer state between Tb^{3+} and the cryptand which leads to nonradiative return to the ground state (Sect. 4.5). Note again the analogy with $YVO_4 : Tb^{3+}$, which also does not luminesce efficiently due to quenching via a charge (or electron) transfer state (Sect. 4.5).

These findings also suggest the way to improvement: Tb^{3+} is to be preferred over Eu^{3+} because its larger gap between the emitting level and the next lower level (see Fig. 2.14) makes its emission less sensitive to the presence of water molecules (compare also Sect. 4.2.1). However, the use of Tb^{3+} will only lead to efficient luminescence if higher excited configurations (like charge-transfer states) are at high energy. This has been realized by using another type of macrocyclic ligand which shields better from the water molecules and does not introduce harmful excited states. This ligand is bpy-branched triazacyclononane [22]. Up till now the maximum quantum efficiencies obtained for these types of complexes are 20% for Eu^{3+} and 40% for Tb^{3+}.

In closing we note that a very different way to realize luminescence immunoassay is the use of commercial phosphors. By using $YVO_4 : Eu^{3+}$, for example, it has been possible to achieve acceptable results. The powder particles are bound to the antibody and are in this way connected to the object of study. The quantum efficiencies are high, and shielding from water molecules is no longer a problem because the luminescent species are in the solid. However, even the finest particles are very large relative to the molecular scale on which the cryptate operates.

Some research is known in which the potential of the luminescence of "caged" rare earth ions was investigated in a very general way. Also zeolites have been included [24]. Zeolites are solid materials which contain internal holes which can contain ions or molecules. They are widely applied in catalysis and their cost is low. Up till now the results on these systems with "caged" ions or molecules are not too promising. Nevertheless it is clear that the use of organic groups as absorbing features has a large advantage over inorganic groups, since their absorption strength is easily one order of magnitude higher.

10.4 Electroluminescence

10.4.1 Introduction

When a luminescent material can be excited by application of an electric voltage, we speak of electroluminescence. In order to convert electric energy from the applied voltage into radiation, three steps have to be considered: excitation by the applied field, energy transport to the luminescent center, and emission from this center. Acoording to the voltage applied, one can distinguish between low-field or high-field electroluminescence. Light-emitting diodes, where energy is injected into a p-n junction, are typical of low-field electroluminescence. The applied voltage is characteristically a few volts. High-field electroluminescence requires electric fields of 10^6 Vcm^{-1}. Materials based on ZnS are popular in this type of electroluminescence. Low-field electroluminescence operates usually with direct current, whereas high-field electroluminescence operates usually with alternating current (ACEL). In this paragraph we will first consider low-field electroluminescence (with applications like light-emitting diodes and laser diodes, also called semiconductor lasers), and subsequently high-field electroluminescence which shows a potential for display (thin-film electroluminescence). For more elaborate treatments the reader is referred to several chapters in a recent book edited by Kitai [25].

10.4.2 Light-Emitting Diodes and Semiconductor Lasers

Semiconductors can be classified as n-type or p-type depending on the nature of the dopant. For our purpose we consider a p-n junction, i.e. the interface between a piece of n-type and a piece of p-type semiconductor. The band structure and the electron distribution around the junction are drawn schematically in Fig. 10.14.

A voltage is applied in such a way that electrons are supplied to the n-type side of the junction (forward bias). As a consequence electrons in the conduction band of the n-type semiconductor fall into the holes of the valence band of the p-type semiconductor (see Fig. 10.15). In certain junctions, depending on the nature

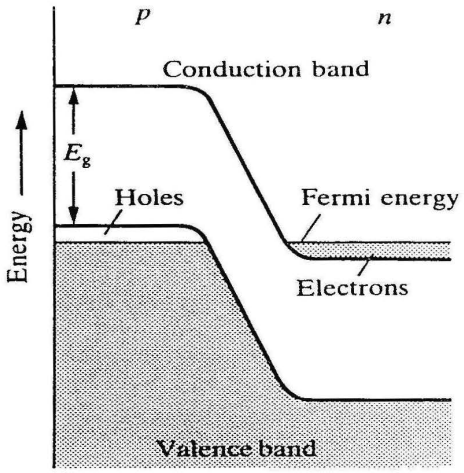

Fig. 10.14. Energy level structure of a p-n junction

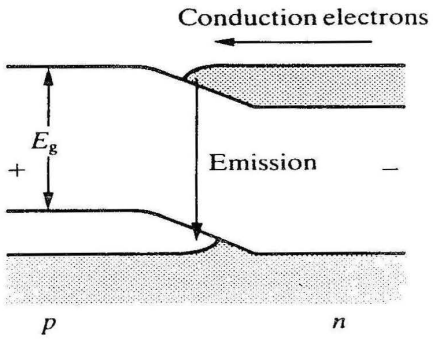

Fig. 10.15. As Fig. 10.14 with applied forward bias. Figs 10.14 and 10.15 are reproduced with permission from Ref. [38]

of the semiconductor, the energy which is involved in this transitions is emitted as radiation. This is especially the case for direct semiconductors which are defined as semiconductors with an optically allowed band-to-band transition. In this way we have obtained a light-emitting diode. These are applied in electronic displays.

Such a light-emitting diode is not yet a laser. However, it is easy to use the radiative electron-hole recombination in a p-n junction as the basis of a laser. Population inversion can be realized by rapidly taking away the electrons which have fallen into the holes of the valence band. These lasers are nowadays widely used (optical communication, compact disc player). An additional large advantage is their small dimension (< 1 mm).

Using GaAs it is easy to produce infrared emission from a p-n junction. The upconversion of this radiation into visible radiation was discussed in Sect. 10.2. By incorporating phosphor in GaAs, the band gap increases and the emission shifts to

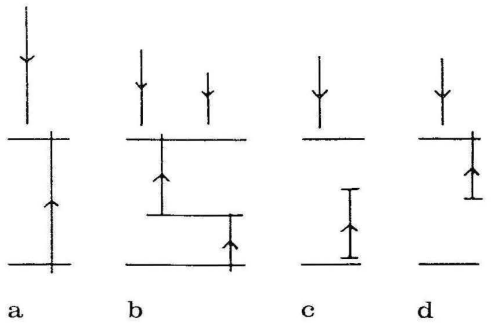

Fig. 10.16. Impact processes in a solid. a: Band-to-band ionization. b: Two-step band-to-band ionization. c: Impact excitation. d: Impact ionization. After J.W. Allen [27]

the visible. For example, $GaAs_{0.6}P_{0.4}$ shows red-light emission, and GaP green. The former is still a direct semiconductor, the latter however is an indirect semiconductor. Since the optical transition is now forbidden, i.e. slow, the radiationless processes become of more importance, so that this diode has a low efficiency.

The semiconductors ZnS and ZnSe have still higher band gaps which decreases the radiative rate further. Also it has been hard to produce n- as well as p-type material. Although some progress has been made, the success of diodes based on II-VI semiconductors is still restricted [26].

10.4.3 High-Field Electroluminescence

The discovery of ACEL in powders by Destriau goes back to 1936. Nevertheless our understanding of the fundamental processes is restricted as reviewed by Allen [27]. This author stresses the analogy between high-field electroluminescence and the phenomena in a gas discharge lamp. In such a lamp, atoms are excited or ionized by impact with energetic electrons which gain energy from an applied voltage (compare also Fig. 6.1 and Sect. 6.2). That the efficiency of such a system can be high, follows from the success of luminescent lighting. The solid-state analogue (high-field electroluminescence) did, however, not bring such high efficiencies.

Electrons (or holes) in a solid can be accelerated by an electric field. However, they can easily lose energy by phonon emission (i.e. by exciting lattice vibrations). Therefore a high field is necessary, so that the gain from the field exceeds the loss to the phonons. Since the path-length in a solid is small, the luminescent center concentration should be high; a limit may be set by concentration quenching. The impact processes to be considered are schematically depicted in Fig. 10.16.

(a) band-to-band impact ionization creates electrons and holes which can recombine radiatively through a luminescent center. The disadvantage is that the current increases very rapidly with voltage (this prevents stable operation), and that the fields required are very high.

(b) in the two-step band-to-band impact ionization, an incident hot carrier ionizes a deep level and then another hot carrier raises an electron from the valence band to the deep level. In this way free electrons and holes are produced. In ZnS and ZnSe, appreciable carrier generation can occur at fields an order of magnitude lower than required for single-step band-to-band ionization. It is attractive to have a high concentration of the impact-ionizable centre and a lower concentration of luminescent centers in order to prevent concentration quenching.

(c) impact excitation of the luminescent center. This seems to be the mechanism for ZnS : Mn^{2+} which is used in commercially available devices. The power efficiency η can be estimated as

$$\eta \sim h\nu\sigma N/eF \tag{10.1}$$

Here F is the electric field, hν the emitted energy, and $(sN)^{-1}$ the distance which a hot electron covers between two impacts (σ is the cross section and N the optimum luminescent center concentration). With the typical values $h\nu = 2$ eV, $s = 10^{-16}$ cm^2, $N = 10^{20}$ cm^{-3}, and $F = 10^6$ Vcm^{-1}, it follows that $\eta \sim 2\%$, in agreement with experiment.

(d) Impact ionization of a luminescent center seems to occur in the electroluminescence of rare-earth doped SrS and CaS.

At the moment it is difficult to see how a considerable improvement in high-field electroluminescence efficiency can be obtained.

In thin-film electroluminescence, a transparent front electrode and an opaque back electrode are used. The former may be a thin layer of indium-tin oxide, the latter a thin layer of aluminium. In the early 1970s a MISIM device (metal-insulator-semiconductor-insulator-metal) with a ZnS : Mn^{2+} electroluminescent layer was shown to maintain bright luminescence for thousands of hours. The insulators can be selected from a large groups of oxides.

The preparation method of the thin layers and the electroluminescent materials available are reviewed in Ref. [28]. Among the techniques used are sputtering, vacuum evaporation, metal-organic chemical-vapor deposition (MOCVD) and atomic layer epitaxy (ALE).

The most successful material is ZnS : Mn^{2+}. Its emission has a yellow colour (see also Fig. 10.17). The transition involved is the well-known $^4T_1 - {}^6A_1$ transition (Sect. 3.3.4c). The optimum Mn concentration is about 1 mole %.

In order to realize multicolor electroluminescent devices there has been world-wide research into other materials. None has been found to be as efficient as ZnS : Mn^{2+}. As examples, we can mention ZnS : LnF^{3+} (Ln = rare earth) films where, for example, Ln = Tb^{3+} gives green and Ln = Sm^{3+} red electroluminescence, and MS(M = Ca,Sr) : Ce^{3+} or Eu^{2+} (green and red emission, respectively). Many other proposals can be found in the literature.

Thin-film electroluminescent (TFEL) devices can be used for display purposes [29]. Since 1983, Helsinki airport uses such a display based on ZnS:Mn^{2+} in the arrival hall. At the moment multi-color devices are being brought out on the market, and are expected to take about 5% of the flat-panel display market in the coming years (the greater part still being color liquid-crystal displays). The red and green

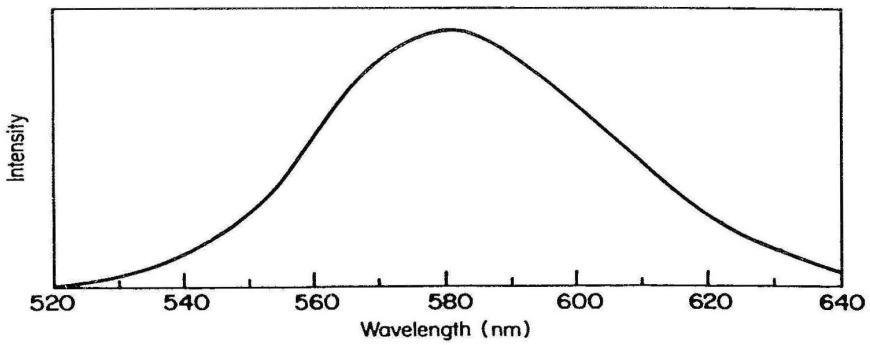

Fig. 10.17. The electroluminescence emission spectrum of ZnS : Mn^{2+}

are produced by the emission of ZnS : Mn^{2+} using filters (compare Fig. 10.17). The problem is in the blue, and a good material is still lacking. The SrS : Ce films seem to be the best solution to fill in the gap. More recently cerium-activated alkaline earth thiogallates were proposed [29].

10.5 Amplifiers and Lasers with Optical Fibers

The first lasers with optical fibers were proposed in 1964 and realized in 1974 [30]. For a few years this field of application has been exploding, since large successes were obtained in the production of useful amplifyers in the spectral area around 2 μm, a wavelength of recognised interest for long- and medium-distance optical communication. Silica fibers doped with Er^{3+} are commercially available for this purpose.

Because we are concentrating the discussion on the Er^{3+} ion, its energy level scheme, as far of importance, is given in Fig. 10.18. The Er^{3+} ion can be pumped with 0.98 or 1.48 μm radiation from a semiconductor laser (Sect. 10.4), i.e. in the $^4I_{15/2} - {}^4I_{11/2}$ or $^4I_{13/2}$ transition, respectively. (Stimulated) emission will occur at 2.5 μm ($^4I_{11/2} \rightarrow {}^4I_{13/2}$) or 1.5 μm ($^4I_{13/2} \rightarrow {}^4I_{15/2}$).

In Sect. 3.6 it was argued that a three-level laser is not so easy to operate as a four-level laser. The reason for this is that a three-level laser requires saturation of the pumping transition, whereas a four-level laser requires only compensation of the optical losses. Fibers, however, have a large advantage over crystals or other bulky materials, viz. their geometric configuration (small diameter and large length). Such a configuration makes it very easy to satisfy laser conditions, even though this is not possible in a bulky sample [30,31].

The interest in Er^{3+}-doped fibers stems from the fact that silica as well as fluoride glasses show very low absorption in the emission region mentioned above (see Fig. 10.19). The silica glasses transmit the $^4I_{13/2} \rightarrow {}^4I_{15/2}$ emission best, the fluoride glasses the $^4I_{11/2} \rightarrow {}^4I_{13/2}$ emission. Figure 10.19 is an absorption spectrum; for

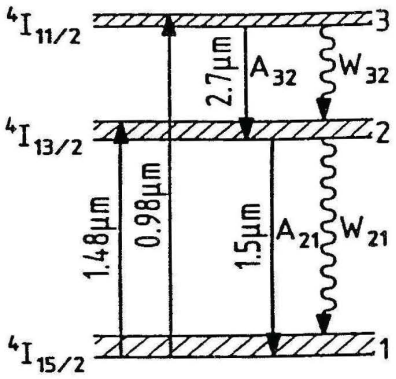

Fig. 10.18. Lower energy level scheme of Er^{3+}. Compare also Table 10.3

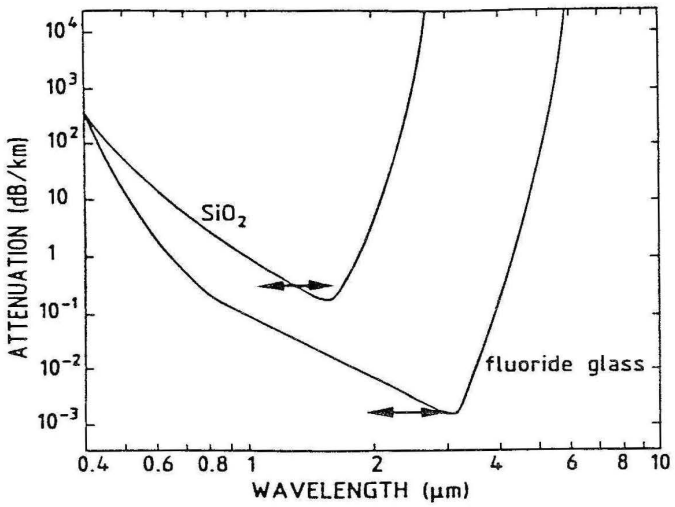

Fig. 10.19. The optical transmission spectra of undoped silica and fluoride glass

fibers the attenuation of the optical signal of a given wavelength is given in dB/km. An emission spectrum of the 2.7 μm $^4I_{11/2} \rightarrow {}^4I_{13/2}$ Er^{3+} emission of ZBLAN : Er^{3+} (compare Sect. 10.1.2c) is given in Fig. 10.20 for bulk and fiber. The considerable narrowing in the case of the fiber points to amplification by stimulated emission.

It is of interest to compare Er^{3+} in silica and in fluoride glass. Some data are given in Table 10.3 where the notation refers to the energy level scheme in Fig. 10.18. The radiative rates are about the same, but the nonradiative ones are very different. The latter is due to the difference between the maximum vibrational frequencies (1100 cm^{-1} for silica glass and 500 c^{m-1} for the fluoride glass) (compare also Sect. 4.2.1). The data show that Er^{3+} in silica will mainly give the $^4I_{13/2} \rightarrow {}^4I_{15/2}$ emission at 1.5 μm. Fluoride glasses will also give the 2.7 μm $^4I_{11/2} \rightarrow {}^4I_{13/2}$ emission.

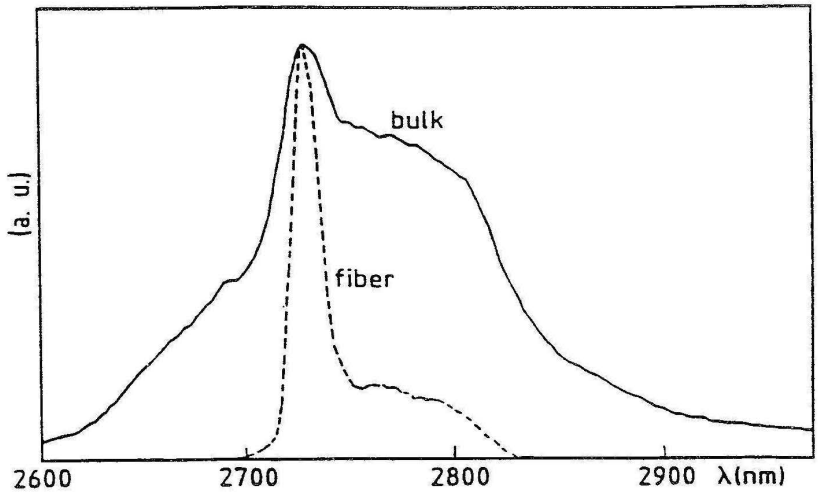

Fig. 10.20. Emission spectrum of a ZBLAN : Er^{3+} glass for a bulk sample and a fiber. After F. Auzel [30]

Table 10.3 Some data on the transitions of Er^{3+} in glasses. Compare also Fig. 10.18

Transition rate		Transition probability (s^{-1})	
Radiative	Nonradiative	Silica	Fluoride
A_{32}		10	10
	W_{32}	10^6	50
A_{21}		100	100
	W_{21}	250	2.10^{-4}

In conclusion, doped optical fibers bring large gains, even for optical transitions which cannot be used for that purpose in a bulk sample. They are now part of telecommunication nets, and most probably cannot be replaced.

10.6 Luminescence of Very Small Particles

The luminescence of small particles, especially of semiconductors, is a fascinating development in the field of physical chemistry, although it is too early to evaluate the potential of these particles for applications. The essential point is that the physical properties of small semiconductor particles are different from the bulk properties and from the molecular properties. It is generally observed that the optical absorption edge shifts to the blue if the semiconductor particle size decreases. This is ascribed to the quantum size effect. This is most easily understood from the electron-in-a-box

model. Due to their spatial confinement the kinetic energy of the electrons increases. This results in a larger band gap.

As an example, we can mention colloids of ZnS. They can be prepared with variable particle size (down to 17-Å diameter, which corresponds to particles containing about 60 molecules of ZnS). The onset of the optical absorption shifts from 334 nm (large particles and bulk) to 288 nm (17-Å particles). The particles show luminescence. Also the emission maximum shifts to shorter wavelength if the particle size is decreased.

A recent, well-defined example of such clusters is the existence of CdS superclusters in zeolites [32]. The authors prepared very small CdS clusters in zeolites. In zeolite Y, for example, there are sodalite cages (5 Å) and supercages (13 Å). Well-defined clusters can be made using these cages. The zeolites were Cd^{2+}-ion exchanged and subsequently fired in H_2S. The resulting zeolite is white (note that CdS is yellow). The products were characterized by several means. It was shown that CdS is within the zeolite pore structure. There are discrete $(CdS)_4$ cubes in the sodalite cages. The cubes consist of interlocking tetrahedra of Cd and S. For high enough CdS concentrations these clusters are interconnected. As this interconnection proceeds, the absorption spectra shift in band edge from 290 to 360 nm. These materials show luminescence. Three different emissions have been observed, viz., a yellow-green one (ascribed to Cd atoms), a red one (ascribed to sulfur vacancies), and a blue one (ascribed to shallow donors). A very interesting aspect is that the vibrational mode responsible for the nonradiative transitions in these materials has a frequency of 500-600 cm^{-1}. This is higher than the highest phonon frequency in CdS. This indicates that interface and host (zeolite) phonons are responsible for these processes.

Recently the same group synthesized a compound $Cd_{32}S_{14}(SC_6H_5)_{36}$. DMF_4 [33]. Its structure contains an 82 atom CdS core that is a roughly spherical piece of the cubic sphalerite lattice $\sim$ 12 Å in diameter. The crystals of this compound emit a green luminescence with a maximum at about 520 nm. The corresponding excitation maximum is at 384 nm. Luminescence spectra at 6.5 K are given in Fig. 10.21.

A comparison of this excitation spectrum with the absorption spectrum of CdS (see Fig. 10.21) shows clearly that the small CdS cluster absorbs at much higher energy than the CdS bulk. Broad band emission from CdS is usually interpreted as luminescence due to defect centers (see Sect. 3.3.9a). However, the CdS core in $Cd_{32}S_{14}(SC_6H_5)_{36}.DMF_4$ has no defects. Herron et al. [33] have ascribed the emission to a charge-transfer transition.

Since bulk CdS shows free-exciton emission at low temperatures [34], it is interesting to compare these results on CdS with the discussion in Sect. 3.3.9b on the transition from semiconductors to insulators. There it was shown that narrow-line free-exciton emission transforms into broad-band localized emission, if the amount of delocalization of the excited state decreases. Since the valence band to conduction band transition of CdS is in principle a $S^{2-} \rightarrow Cd^{2+}$ charge-transfer transition, this would bring the discussion on CdS in line with results from a different origin (see Sect. 3.3.9b). By all means the case of $Cd_{32}S_{14}(SC_6H_5)_{36}.DMF_4$ is a nice example of luminescence research on a well-defined cluster showing the quantum-size effect.

An interesting development in this field is the report by Dameron et al. [35] of the biosynthesis of quantum-sized CdS crystals in the yeast cells Candida glabrata

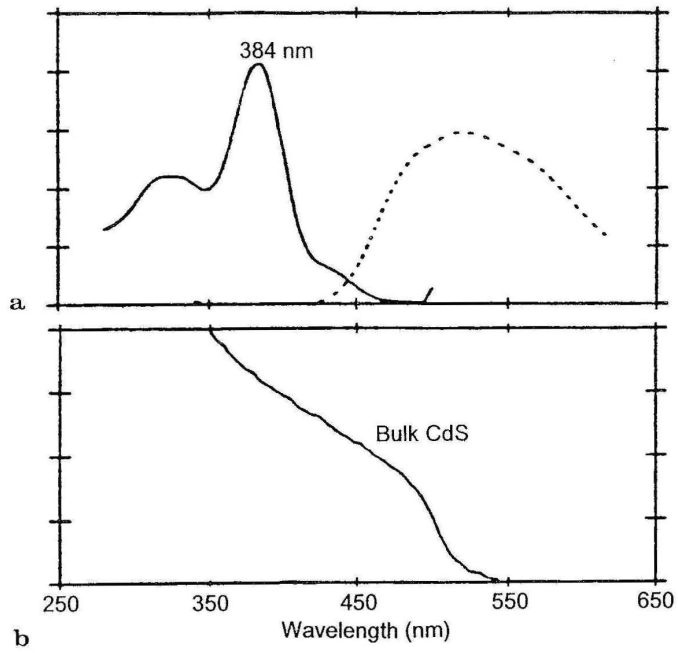

Fig. 10.21. A: Emission (broken line) and excitation spectra of the luminescence of $Cd_{32}S_{14}(SC_6H_5)_{36}.DMF_4$ at 6.5 K. B: Absorption spectrum of bulk CdS. After data in Ref. [33]

and schizosaccharomyces pombe. Exposed to Cd^{2+} ions these cells synthesize certain peptides with an enhanced sulfide production. Small CdS crystals are formed inside the cells. These crystallize in the rock salt structure (and not in the thermodynamically stable hexagonal configuration). The organism controls particle nucleation and growth, so that uniformly sized CdS particles of about 20 Å are formed. They show pronounced quantum-size effects. This is the first example of the biosynthesis of quantum-sized semiconductor crystallites. It constitutes a metabolic route for the detoxification of Cd^{2+}-infected living cells.

No doubt these semiconductor superclusters present a novel class of materials where the three-dimensional structure can be controlled. They present a challenge to synthetic and physical chemists. The most recent developments can be found in Refs [36] and [37].

References

1. Auzel F (1985) In Jezowska-Trzebiatowska B, Lengendziewicz J, Strek W (eds) Rare earth spectroscopy. World Scientific, Singapore, p 502
2. Auzel F (1973) Proc. IEEE 61: 758
3. Auzel F (1966) C.R. Ac. Sci (Paris) 262 :1016 and 263: 819
4. Sommerdijk JL, Bril A (1974) Philips Techn. Rev. 34: 24

5. Blasse G, de Pauw ADM (1970) unpublished
6. Oomen EWJL (1991) Adv. Mater. 3: 403
7. Ouwerkerk M (1991) Adv. Mater. 3: 399
8. Genet M, Huber S, Auzel F (1981) C.R. Ac. Sci. (Paris) 293: 267
9. DeKalb EL, Fassel VA (1979) In Gschneidner Jr KA, Eyring L (eds) Handbook on the physics and chemistry of rare earths Holland, Amsterdam, chap 37D; D'Silva AP, Fassel VA (1979) ibid. chap 37E
10. de Vries AJ, Smeets WJJ, Blasse G (1987) Mat. Chem. Phys. 18: 81
11. de Haart LGJ, Blasse G (1986) J. Solid State Chem. 61: 135
12. Blasse G (1968) J. Inorg. Nucl. Chem. 30: 2091
13. Boulon G (1987) Mat. Chem. Phys. 16: 301
14. Durville F, Champignon B, Duval E, Boulon G (1985) J. Phys. Chem. Solids 46: 701
15. Blasse G (1990) Adv. Inorg. Chem. 35: 319
16. Basun SA, Kaplyanskii AA, Feofilov SP (1992) Sov. Phys. Solid State 34: 1807
17. Tallant DR, Wright JC (1975) J. Chem. Phys. 63: 2074
18. Draai WT, Blasse G (1974) Phys. Stat. Sol.(a) 21: 569
19. Lammers MJJ, Blasse G (1986) Chem. Phys. Letters 126: 405; Berdowski PAM, Lammers MJJ, Blasse G (1985) J. Chem. Phys. 83: 476
20. Hazenkamp MF, Blasse G (1990) Chem. Mater. 2: 105
21. Hazenkamp MF, Blasse G (1992) J. Phys. Chem. 96 :3442; (1993) Research Chem. Intermediates 19: 343
22. Sabbatini N, Guardigli M, Lehn JM (1993) Coord. Chem. Revs 123 :201; Sabbatini N, Guardigli M (1993) Mat. Chem. Phys. 31: 13
23. Soini E, Hemmila I (1979) Clin. Chem. 25 :353
24. Bredol M, Kynast U, Ronda C (1991) Adv. Mater. 3: 361
25. Kitai AH (ed) (1993) Solid state luminescence. Chapman and Hall, London
26. Walker CT, DePuydt JM, Haase MA, Qiu J, Cheng H (1993) Physica B185 :27
27. Allen JW (1991) J Luminescence 48,49: 18; Chadha SS (1993) chap 6 in Ref. [25]
28. Leskelä M, Tammenmaa M (1987) Mat. Chem. Phys. 16: 349; Müller GO (1993) chap 5 in Ref. [25]
29. Morgan N (1993) Opto and Laser Europe 4 (March) p 26; (July) p 29; Mach R (1993) chap 7 in Ref. [25]
30. Auzel F (1993) In: Proceedings int. conf. defects insulating materials, Nordkirchen. World Scientific, Singapore, p 39; Snitzer E (1994) J. Luminescence, 60/61:145
31. Yen WM (1989) In Jezowska-Trzebiatowska B, Legendziewicz J, Strek W (eds) Excited states of transition metal elements. World Scientific Singapore, p 621
32. Herron N, Wang Y, Eddy MM, Stuckey GD, Cox DE, Moller K, Beitz T (1989) J. Am. Chem. Soc. 111 :530; Wang Y, Herron N (1988) J. Phys. Chem. 92: 4988
33. Herron N, Calabrese JC, Farneth WE, Wang Y (1993) Science 259: 1426
34. See, for example, Shionoya S (1966) In: Goldberg P (ed) Luminescence of inorganic solids. Academic New York, p 205
35. Dameron CT, Reese RN, Mehra RK, Kortan AR, Carroll PJ, Steigerwalt ML, Bras LE, Winge DR (1989) Nature (London) 338: 596
36. Bawendi MG, Carroll PJ, Wilson WL, Brus LE (1994), J. Chem. Phys. 96:946
37. Bhargava R, Gallagher D, Welker T (1994) J. Luminescence 60/61:275; Bhargava R, Gallagher D, Hong X, Nurmikko A (1994) Phys. Rev. Letters 72:416
38. Atkins PW (1990) Physical chemistry. Oxford University Press, Oxford, 4th ed

Appendix 1. The Luminescence Literature

The present text has clearly the character of an introduction into the field. Those who want to know more or to keep up with the luminescence literature do not have an easy task, since this literature is widely spread. The suggestions which follow originate from the authors experience and personal preference.

Books

– A.H. Kitai, editor, Solid State Luminescence; Theory, materials and devices, Chapman and Hall, London, 1993. A multi-authored book on many topics in the field of luminescence and luminescent materials. Many topics are discussed; the stress on electroluminescence is strong.

– B. Henderson and G.F. Imbusch, Optical Spectroscopy of Inorganic Solids, Oxford Science Publication, Clarendon Press, Oxford, 1989. An extensive treatment of luminescent centers in solids. Chapters on color centers, lasers and experimental techniques are included.

– S.W.S. McKeever, Thermoluminescence of Solids, Cambridge University Press, Cambridge, 1985. An excellent treatment of thermoluminescence and related phenomena.

– Proceedings of the Summer Schools on Spectroscopy in Erice (Sicily) edited by B. Di Bartolo and published by Plenum Press, New York. The first one dates from 1975; there has been a continuation every two years. Each book contains several chapters at an advanced level on all possible topics of spectroscopy and luminescence and (to a less extent) materials.

– Mat. Chem. Phys. 16 (1987) no. 3-4, a special issue devoted to new luminescent materials edited by G. Blasse. This issue contains several review papers with a stress on materials (X-ray phosphors, lamp phosphors, glasses, and electroluminescent thin films).

– K.H. Butler, Fluorescent Lamp Phosphors, The Pennsylvania State University Press, University Park, 1980. Interesting for its historical and application chapters. The book does not include the developments after the introduction of the rare earth phosphors.

– L. Ozawa, Cathodoluminescence, VCH, Weinheim, 1990.

– T. Hase, T. Kano, E. Nakazawa and H. Yamamoto, Phosphor Materials for Cathode-Ray Tubes, in Adv. Electr. Electron Physics (Ed. P.W. Hawkes) 79 (1990) 271. The latter two texts describe the theory and application of cathode-ray luminescence.

– Heavy Scintillators for Scientific and Industrial Applications (Eds F. De Notaristefani, P. Lecoq and M. Schneegans), Editions Frontières, Gif-sur-Yvette, 1993; proceedings of the workshop Crystal 2000. A good overview of the state-of-the-art in the scintillator field.

Journals

The Journal of Luminescence publishes fundamental papers on luminescence. Interesting are the issues which contain the proceedings of the International Conference on Luminescence (every three years) and of the Dynamics of the Excited State (DPC) meetings (every two years). A large number of relatively short papers show the state-of-the-art in the total field of luminescence throughout the years.

Many other fundamental papers in the field of luminescence can be found in the journals on solid state physics. Here we can mention Physical Review B (USA), Journal of Physics: Condensed Matter (UK), Journal of Physics and Chemistry of Solids, Journal of Experimental and Theoretical Physics (Russia), Physica Status Solidi (Germany).

The field of luminescent materials used to be covered by the Journal of the Electrochemical Society. This has changed completely. Such papers may nowadays be found in journals like the Journal of Solid State Chemistry, Materials Research Bulletin, Chemistry of Materials (USA), Journal of Materials Chemistry (UK), Journal of Materials Science, Japanese Journal of Applied Physics, and Journal of Alloys and Compounds. The latter journal publishes the proceedings of the international rare-earth conferences with many papers on the spectroscopy and luminescence of rare-earth containing materials.

The patent literature is left out of consideration.

Appendix 2. From Wavelength to Wavenumber and Some Other Conversions

Consider an optical center with two energy levels with energies E_1 and E_2 ($E_2 > E_1$). The center can be excited from the lower to the higher level by absorption of radiation. The frequency ν of this radiation is given by the well-known relation $\Delta E = E_2 - E_1 = h\nu$. The frequency is expressed in the unit s^{-1} (the number of vibrations per second). Spectroscopists more often use the wavenumber $\tilde{\nu} = \frac{\nu}{c}$ where c is the velocity of light. The unit of $\tilde{\nu}$ is cm^{-1}. Note that both ν and $\tilde{\nu}$ are linearly proportional to the energy.

Spectrometers often use the wavelength (λ) of the radiation. The wavelength follows from another well-known relation, viz. $\nu\lambda = c$. The wavelength is expressed in nm (10^{-9} m) or mm (10^{-6} m). Note that λ is not proportional to the energy.

Table A.2.1 gives for radiation of a given energy the color, wavelength, wavenumber and frequency. The visible area corresponds to $400 < \lambda < 700$ nm; ultraviolet radiation has $\lambda < 400$ nm, infrared radiation $\lambda > 700$ nm. In wavenumbers these regions are indicated as follows: $14.300 < \tilde{\nu} < 25.000\ cm^{-1}$ is visible, $\tilde{\nu} > 25.000\ cm^{-1}$ is ultraviolet, and $\tilde{\nu} < 14.300\ cm^{-1}$ is infrared.

Semiconductor physics often uses the electron volt (eV) as a measure of energy: 1 eV is the energy acquired by an electron when it is accelerated through a potential difference of 1 V. The energy of 1 eV corresponds to $8065.5\ cm^{-1}$.

Table A.2.1. Conversion of spectral units for radiation of certain colors.

Wavelength λ (nm)	Frequency $\nu(10^{14}s^{-1})$	Wavenumber $\tilde{\nu}(10^3 cm^{-1})$	Energy (eV)	Colour
1000	3.0	10.0	1.24	infrared
700	4.3	14.3	1.77	red
620	4.8	16.1	2.00	orange
580	5.2	17.2	2.14	yellow
530	5.7	18.9	2.34	green
470	6.4	21.3	2.64	blue
420	7.1	23.8	2.95	violet
300	10.0	33.3	4.15	near ultra-violet
200	15.0	50.0	6.20	far ultra-violet

Appendix 3. Luminescence, Fluorescence and Phosphorescence

Those who start to read the literature on luminescence are often surprised by the variation of the terminology. Luminescence is the general term of the phenomenon. We have used it in this book generally. In this way one avoids using the wrong term. The terms fluorescence and phosphorescence are especially popular among those working on carbohydrates. Fluorescence is a spin-allowed transition ($\Delta S = 0$) which is very fast, whereas phosphorescence is a spin-forbidden transition ($\Delta S = 1$) which is very slow. In compounds of the lighter elements, like carbohydrates, the spin-orbit coupling is very weak. Therefore the spin quantum numbers are good quantum numbers, i.e. there is no mixing of importance between $S = 0$ and $S = 1$ states, and the spin-selection rule is strict. In this way it is easy to distinguish between fluorescence and phosphorescence.

The terms fluorescence and phosphorescence are often used for heavier elements too. This is sometimes legitimate. For example, the $^2E \rightarrow {}^4A_2$ emission of Cr^{3+} (Sect. 3.3.4) can be called phosphorescence, and the $^4T_2 \rightarrow {}^4A_2$ emission fluorescence. The $^5D_0 - {}^7F_J$ emission of Eu^{3+} (Sect. 3.3.2.) can be called phosphorescence. It is definitely wrong to call the $^2E - {}^4A_2$ emission of Cr^{3+}, or the $^5D_0 - {}^7F_J$ emission of Eu^{3+} fluorescence, although this is frequently done. Nevertheless we prefer to call all these emissions luminescence. Actually, the $^4T_2$ L $^4A_2$ emission of Cr^{3+} is not an allowed transition, because of the parity selection rule, nor is the slow rate of the $^5D_0 - {}^7F_J$ emission of Eu^{3+} in the first place due to the spin-selection rule (the parity selection rule is of more importance in this case).

To increase the confusion, some authors use the word phosphorescence when they mean afterglow (Sect. 3.4). It will be clear that phosphorescence characterizes a specific emission transition (i.e. $\Delta S = 1$, slow), whereas afterglow relates to whatever type of emission transition after trapping of an electron or hole elsewhere.

Garlick [1] proposed, long ago, the sole use of the terminology as summarized here.

Reference

1. Garlick GFJ (1958) In: Flügge S (ed) Handbook der Physik, Springer, Berlin Heidelberg New York, Vol XXVI, p 1

Appendix 4. Plotting Emission Spectra

Experimental data on luminescent emission spectra are usually presented as relative emitted energy per constant wavelength interval, i.e. Φ_λ vs λ. Usually the maximum of this curve is considered to be the peak of the emission band.

For theoretical considerations, however, it is imperative to plot the relative emitted energy per constant energy interval, i.e. Φ_E vs E. As shown in appendix 2, the frequency (ν) or wavenumber ($\tilde{\nu}$) can also be used, since they are proportional to E. The Φ_E vs E spectrum yields a value of E for Φ_E (maximum) which is not equal to the value of E which is obtained by taking the λ value for Φ_λ (maximum) and converting it to E. In the literature this is often overlooked. A simple example for illustration: if the maximum of an emission band in the Φ_λ vs λ spectrum is at 500 nm, the emission maximum is not at $\tilde{\nu} = 20.000\ \mathrm{cm}^{-1}$, but at a lower $\tilde{\nu}$. This can be seen as follows.

Φ_λ and Φ_E are related to each other by the equation

$$\Phi_E = \Phi_\lambda\ \lambda^2 (hc)^{-1} \qquad \text{(A 4.1)}$$

Here c is the velocity of light, and h the Planck constant. Eq.(A 4.1) can be easily derived by remembering that in the Φ_λ vs λ spectrum we plot per wavelength interval $d\lambda$, i.e. we plot $\Phi_\lambda d\lambda$. In order to convert $d\lambda$ to an energy interval dE, the expression $E = hc\lambda^{-1}$ is used. By differentiation it follows that $dE = hc\lambda^{-2}d\lambda$.

As a matter of fact the maxima in the Φ_λ vs λ and Φ_E vs E spectra coincide within the experimental error in the case of sharp lines. However, in the case of broad bands they are different. Only in the Φ_E vs E plot a broad emission band is expected to show a Gaussian shape. Figure A 4.1 illustrates these effects for a simple example. The literature can be found in, for example, ref. [1]. It is self-evident, that eq. (A 4.1) should not be used for excitation spectra.

References

1. Curie D, Prener JS (1967) In: Aven M, Prener JS (eds) Physics and chemistry of II-VI compounds. North Holland, Amsterdam, chap 9
2. Blasse G, Verhaar HCG, Lammers MJJ, Wingefeld G, Hoppe R, de Maayer P (1984) J. Luminescence 29 :497.